



Numerical Investigation of Low Speed Performance of Transonic Coflow Jet Supercritical Airfoil

Jeremy Boling*, Subash Dhakal†, Yunchao Yang‡ and Ge-Cheng Zha§
 Department of Mechanical and Aerospace Engineering
 University of Miami, Coral Gables, Florida 33124
 E-mail: gzha@miami.edu

This paper studies the low-speed performance of coflow jet (CFJ) supercritical airfoils based on three baseline supercritical airfoil of NASA SC(2)-1010, RAE-2822, and NASA SC(2)-0714. The simulations employ the intensely validated in-house CFD solver, FASIP, using Reynolds Averaged Navier-Stokes(RANS) equations with one-equation Spalart-Allmaras turbulence model. Numerical studies are carried out to investigate the effects of slots location and size, airfoil thickness, and jet intensity on the low speed performance of the airfoil. It is found that for the CFJ supercritical airfoils, very high maximum lift coefficient is obtained while improving the aerodynamic efficiency at cruise at low angle of attack(AoA). This study indicates that the CFJ-NASA-SC(2)-0714 supercritical airfoil is able to achieve super-lift coefficient of 9.1 at Mach 0.1, attributed to its large leading edge radius and airfoil thickness. Whereas the CFJ-RAE-2822 and CFJ-NASA SC(2)-1010 airfoils achieve lower maximum lift coefficient of 5.4 and 5.9 respectively. The overall low speed performance of supercritical CFJ airfoils is significantly superior to conventional super-critical airfoils. The results are very encouraging to achieve high lift coefficient for takeoff/landing without using the conventional flap systems.

Nomenclature

V	Flow Velocity
ρ	Air Density
α, AoA	Angle of Attack
\dot{m}	Mass Flow Rate
M	Mach Number
M_i	Isentropic Mach Number
Re	Reynolds Number
L	Aerodynamics Lift
D	Aerodynamic Drag
p	Static Pressure
p_0	Total Pressure
η	Pumping Power
q_∞	Freestream Dynamics Head, $\frac{1}{2}\rho_\infty V_\infty^2$
C_L	Lift Coefficient, $\frac{L}{q_\infty S}$
C_{LMAX}	Maximum Lift Coefficient
C_D	Drag Coefficient, $\frac{D}{q_\infty S}$
C_M	Moment Coefficient, $\frac{M}{q_\infty S c}$
C_p	Pressure Coefficient, $\frac{p-p_\infty}{q_\infty}$
C_μ	Jet Momentum Coefficient, $\frac{\dot{m}_j v_j}{q_\infty S}$

*Graduate Research Assistant

†Former Graduate Student

‡PhD Candidate, AIAA Student Member

§Professor, AIAA Associate Fellow

Approved for public release; distribution is unlimited.

$(\frac{L}{D})$	Conventional Aerodynamic Efficiency
P_c	Power Coefficient, $\frac{L}{q_\infty S V_\infty}$
$(\frac{L}{D})_c$	Corrected Aerodynamic Efficiency for CFJ Airfoil, $\frac{L}{D+P/V_\infty} = \frac{C_L}{C_D+P_c}$
$(\frac{C_L^2}{C_D})$	Productivity Efficiency Coefficient
$(\frac{C_L^2}{C_D})_c$	Corrected Productivity Efficiency Coefficient for CFJ Airfoil
∞	Free Stream Conditions
j	Jet Conditions
<i>ESTOL</i>	Extremely Short Takeoff and Landing

I. Introduction

I.A. Background

The supercritical airfoil invented by Whitcomb and his colleagues in NASA¹ in 1960's was a crucial milestone in transonic aerodynamics and technology development. The invention significantly extends drag-rise Mach number towards above 0.8 while maintaining excellent subsonic performance. Recently, Liu and Zha² applied coflow jet (CFJ) active flow technique to a transonic super-critical airfoil RAE2822 and were able to substantially increase the cruise lift coefficient and aerodynamic efficiency at the same time. The productivity efficiency defined by C_L^2/C_D is increased by about 36%. The productivity efficiency is used to measure the maximum capacity of aircraft to transport a gross weight with a certain distance, $R \times W$, where R stands for the maximum range and W stands for the aircraft gross weight.³ Even though the supercritical CFJ airfoil demonstrates a very promising performance at cruise, it is not clear how they behave at low speed for takeoff and landing.

The purpose of this paper is to investigate the low speed performance of supercritical CFJ airfoil for aircraft takeoff/landing performance, including the maximum lift coefficient and the ratio of lift to drag. Aircraft need high lift coefficient at low speed of takeoff/landing phase to compensate the low dynamic pressure. A high C_{Lmax} and L/D at low speed is very desirable to reduce takeoff/landing distance and energy consumption. Extremely Short Takeoff and Landing (ESTOL) performance becomes more and more important to increase airport capacity and meet the rapidly growing air travel population.

Multi-element flap systems have been used as high lift device since WWII. They are very complicated and expensive to make with up to 6% or more of the total aircraft manufacturing cost. For a large transonic transport, the high lift flap system can have over 5000 parts and have a weight of 3.5% to 5% of the aircraft gross weight.⁴ Although a necessity given the lifting requirements at takeoff and landing, they increase weight and thus, fuel consumption at cruise. Furthermore, the C_{Lmax} that conventional flap systems can achieve is in the order of 1.5 to 1.8, not sufficient to achieve ESTOL performance.

In the NASA Technical Paper by Harris⁵, a matrix of different supercritical airfoils are provided with the thickness-to-chord ratio ranging from 2 to 18 percent and lift coefficients from 0 to 1.0. These airfoils were designed as part of NASA's effort to develop airfoils with high transonic cruise efficiency while obtaining good low-speed characteristics. Two airfoils with the thickness of 10% and 14% are selected from NASA's database⁵ as the baseline airfoil to be compared with the CFJ airfoil. One is NASA SC(2)-1010 airfoil and the other is NASA SC(2)-0714 airfoil. The interest for NASA SC(2)-1010 airfoil is that it has high cruise lift coefficient. The interest for NASA SC(2)-0714 airfoil is that it is a widely used airfoil by transonic transports including Boeing 777, C-17, and Airbus A-330/340.⁶ Supercritical airfoil RAE-2822 is chosen as another comparison based on the maximum thickness of 12.1% which falls in between NASA SC(2)-0714 and NASA SC(2)-1010. In addition to each airfoil being of different maximum thicknesses, they all have different leading edge sharpness. The nose of an airfoil can be defined by an elliptic or circular radius depending on the design. Traditional NACA 4-digit airfoils have blunt, circular shapes. This carries over to both NASA SC(2)-1010 and NASA SC(2)-0714 airfoils. RAE-2822 is thicker than than NASA SC(2)-1010, but has a smaller leading edge radius. The sharpness exhibits different behavior at higher angles of attack than the larger radii of the other airfoils studied.

It is appealing to achieve very high maximum lift coefficient at low speed without using flaps, in particular if the same system can be also used for high efficiency transonic cruise. The conducted trade studies in this paper of low-speed, supercritical CFJ airfoils is an effort toward this goal.

I.B. CFJ Active Flow Control

CFJ airfoil is a zero-net mass-flux(ZNMF) active flow control technique developed by Zha et al.,^{2,3,7-17} which has the ability to provide increase in lift and aerodynamic efficiency at low energy expenditure. An injection slot near the leading edge and a suction slot near the trailing edge are used as shown in Figure 1. With the help of a pumping system inside the airfoil, a small amount of air from near the trailing edge is sucked in and energized flow is injected near leading edge in a direction tangent to the main flow. The process does not add any mass flow and hence is a ZNMF system. This technique works by energizing the boundary layer and hence increasing circulation, augmenting lift while decreasing pressure drag due to enhanced leading edge suction and filled wake.

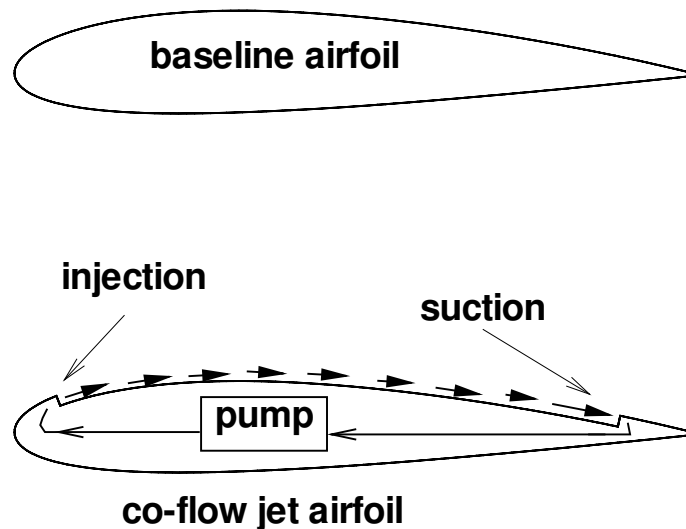


Figure 1: The sketch of a baseline airfoil and a CFJ airfoil.

II. Methodology

II.A. Numerical Approach

The in-house computational fluid dynamics(CFD) code Flow-Acoustics-Structure Interaction Package(FASIP) is applied to conduct the numerical simulations. The Reynolds averaged Navier-Stokes(RANS) equations with one-equation Spalart-Allmaras(SA)¹⁸ turbulence model is used for this research. The low diffusion E-CUSP scheme suggested by Zha et al.¹⁹ and Roe's flux difference scheme²⁰ with the 3rd order weighted essentially non-oscillatory(WENO) scheme are utilized to evaluate the inviscid fluxes. The 2nd order central differencing method is used for the viscous terms discretization. The implicit Gauss-Seidel(GS) line relaxation with two alternative sweeping direction in each time step is applied to achieve a fast convergence rate.²³ Parallel computing is implemented to save wall clock simulation time.²⁴ The code is extensively validated with various transonic flows including CFJ airfoil flows.^{2,11,24-27}

II.B. CFJ Airfoil Parameters

II.B.1. Drag and Lift

Zha et al.⁹ give the following formulations to calculate the lift and drag due to CFJ effect for CFD simulation

$$R_x = (\dot{m}_j V_{j1} + p_{j1} A_{j1}) \cos(\theta_1 - \alpha) - (\dot{m}_j V_{j2} + p_{j2} A_{j2}) \cos(\theta_2 + \alpha) \quad (1)$$

$$R_y = (\dot{m}_j V_{j1} + p_{j1} A_{j1}) \sin(\theta_1 - \alpha) + (\dot{m}_j V_{j2} + p_{j2} A_{j2}) \sin(\theta_2 + \alpha) \quad (2)$$

where x and y represent the drag and lift direction respectively, subscripts 1 and 2 stand for the injection and suction, θ_i ($i = 1, 2$) is the angle between the injection or suction slot surface and the line normal to the airfoil chord, and α is the AoA, as shown in Figure 2.

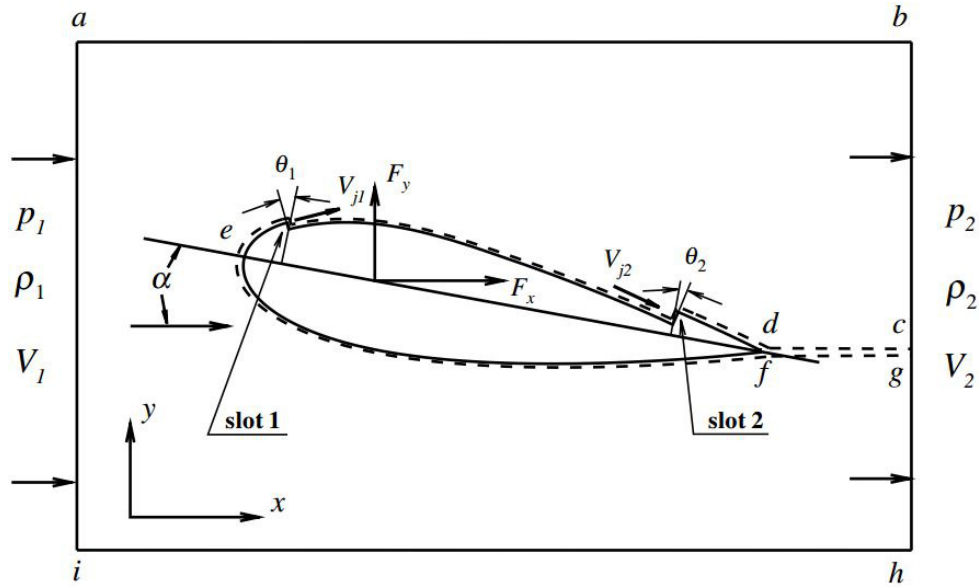


Figure 2: The CFJ airfoil control volume schematic.

The total drag and lift of the CFJ airfoil can then be expressed as below

$$D = F_x - R_x \quad (3)$$

$$L = F_y - R_y \quad (4)$$

where F_x and F_y are the drag and lift force due to surface integral of pressure and shear stress. The corresponding drag and lift coefficients are expressed as following

$$C_D = \frac{D}{\frac{1}{2} \rho_\infty V_\infty^2 S} \quad (5)$$

$$C_L = \frac{L}{\frac{1}{2} \rho_\infty V_\infty^2 S} \quad (6)$$

where ρ_∞ and V_∞ denote the free stream density and velocity. S is the wing planform area. For 2-D airfoil study, S denotes the planform area per unit span, which is equal to the airfoil chord length.

The maximum lift coefficient for potential flow is imposed by the Kutta-condition which does not reflect physical limits when adding energy to the flow via active flow control.

$$C_{Lmax} = 2\pi(1 + t/c) \quad (7)$$

With active flow control, there seems to be no law written for maximum lift coefficient, and anything breaking traditional limits is known as "Super-Lift".

II.B.2. Jet Momentum

The jet momentum coefficient C_μ is a parameter used to quantify the jet intensity, which is defined as

$$C_\mu = \frac{\dot{m}V_j}{\frac{1}{2}\rho_\infty V_\infty^2 S} \quad (8)$$

where \dot{m} is the injection mass flow rate, V_j is the averaged injection velocity at the injection slot opening.

II.B.3. Power Consumption

The CFJ can be implemented by mounting a pumping system inside the wing that withdraws air from the suction slot and blows it into the injection slot. The power consumption can be determined by the jet mass flow and total enthalpy change as follows

$$P = \dot{m}(H_{01} - H_{02}) \quad (9)$$

where H_{01} and H_{02} are the total enthalpy in the injection cavity and suction cavity, respectively. P is the power required by the pump. Introducing the pump efficiency η and total pressure ratio of the pump $\Gamma = \frac{P_{01}}{P_{02}}$, the power consumption can be expressed as

$$P = \frac{\dot{m}C_p T_{02}}{\eta} (\Gamma^{\frac{\gamma-1}{\gamma}} - 1) \quad (10)$$

where γ is the specific heat ratio for air. The power consumption can be further normalized as a power coefficient

$$P_c = \frac{P}{\frac{1}{2}\rho_\infty V_\infty^3 S} \quad (11)$$

II.B.4. Aerodynamic Efficiency

The conventional airfoil aerodynamic efficiency is defined as

$$\left(\frac{L}{D}\right) = \frac{C_L}{C_D} \quad (12)$$

For the CFJ airfoil, the ratio above represents the pure aerodynamic relationship between lift and drag. Taking into account the energy consumption of the CFJ, the conventional aerodynamic efficiency is modified by converting the power consumption into a corresponding drag force. The equation of the corrected aerodynamic efficiency is given as follows¹⁴

$$\left(\frac{L}{D}\right)_c = \frac{L}{D + \frac{P}{V_\infty}} \quad (13)$$

in which the pump power consumption P is converted into a force $\frac{P}{V_\infty}$ added to the aerodynamic drag D . The formulation above can be further expressed using the non-dimensional coefficients C_L , C_D and P_c as

$$\left(\frac{L}{D}\right)_c = \frac{C_L}{C_D + P_c} \quad (14)$$

Note that when the pumping power is set to 0, $\left(\frac{L}{D}\right)_c$ returns to conventional aerodynamic efficiency definition.

A new parameter, the productivity coefficient was introduced by Yang et al.³ It describes the the capability to transport a gross weight for maximum distance at cruise.

$$\left(\frac{C_L^2}{C_D}\right)_c = \frac{C_L^2}{C_D + P_c} \quad (15)$$

III. Results and Discussions

III.A. Validation and Mesh Refinement

The super-critical airfoil NASA(SC)-2 0714 has been used to validate the code as the experimental data for NASA(SC)-2 1010 airfoil is not available. Corrected values of different angles of attack and free stream mach number equal to 0.701 are used as suggested by Rivers et al.²⁸ with free stream $Re = 6 \times 10^6$. The difference between the experimental and CFD coefficient of lift and drag are shown in Figure 3. The maximum difference in C_D is 30.5% and C_L is 10.9% between experimental and numerical results. Figure 4 shows that the predicted airfoil surface pressure distributions C_p agree very well with the experimental results. Table 1 shows the values of lift and drag coefficient for different mesh sizes for the NASA (SC)-2 1010 airfoil. The 601×151 mesh is used for all studies done in this paper.

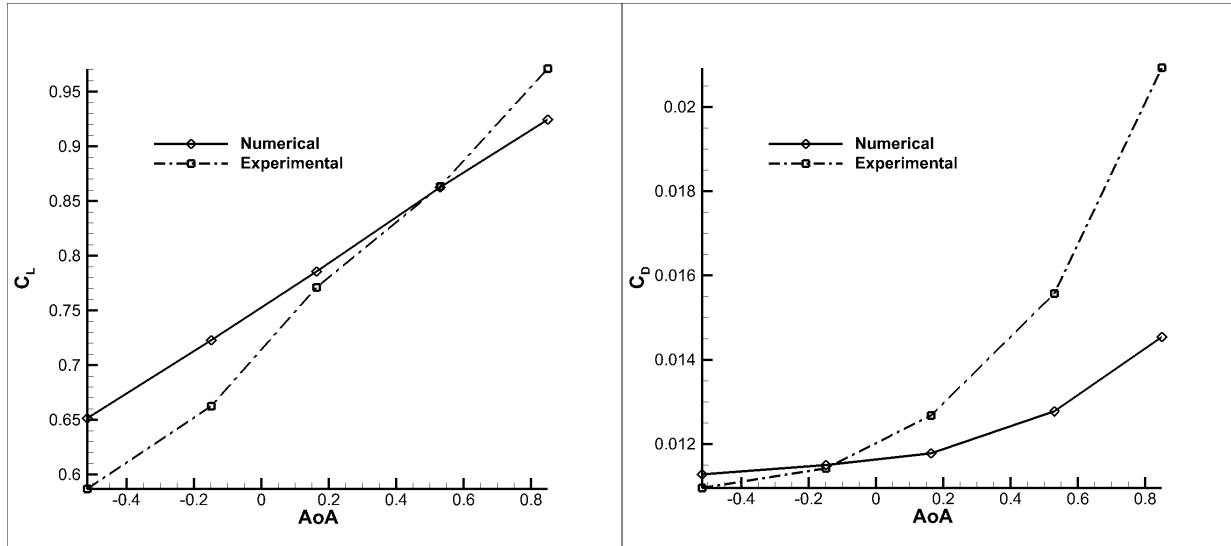


Figure 3: Comparison of lift and drag coefficients between simulation and experiment at $M=0.701$ at different values of angle of attack for NASA SC(2)-0714 airfoil.

Table 1: CFJ airfoil aerodynamic coefficients comparison between different mesh sizes for NASA SC(2)-1010 airfoil at $M=0.701$, $\alpha = 1^\circ$.

Cases	C_L	C_D	C_M	P_C
251×101 mesh	1.519	0.0493	-0.254	0.0087
601×151 mesh	1.483	0.0516	-0.242	0.0071

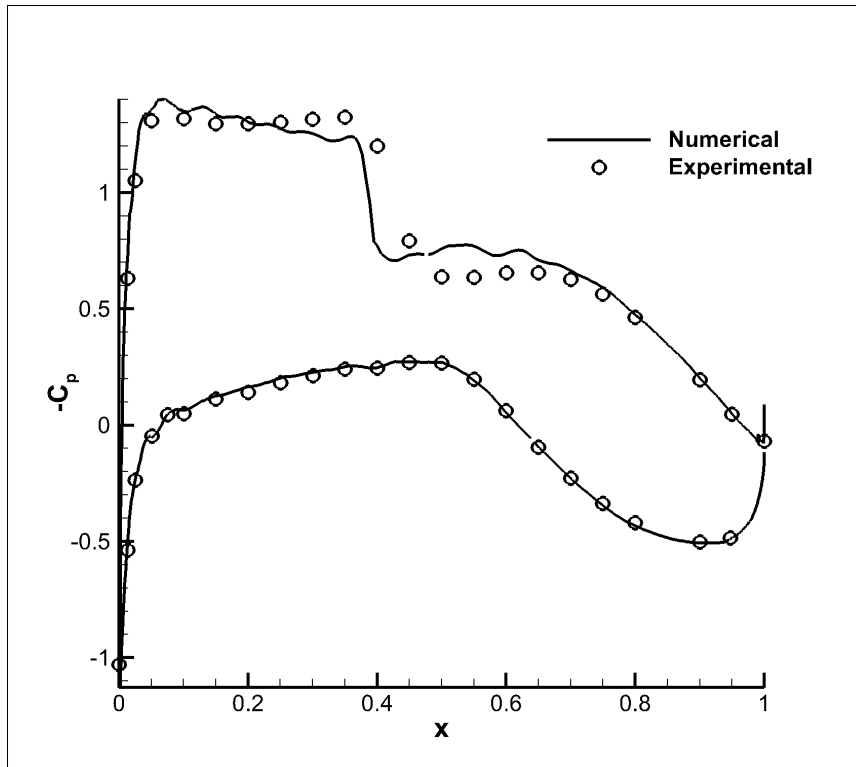


Figure 4: Comparison of pressure coefficients between simulation and experiment at $M=0.701$, $\alpha = 0.53^\circ$ for NASA SC(2)-0714 airfoil

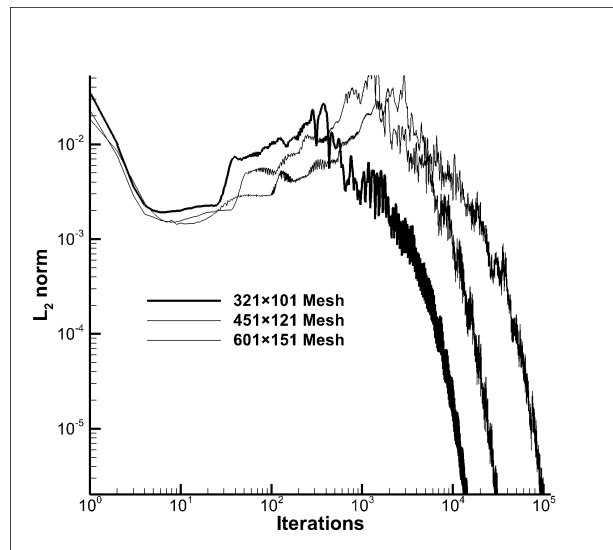


Figure 5: The convergence history of L_2 Norm relative error for NASA SC(2)-0714 baseline airfoils.

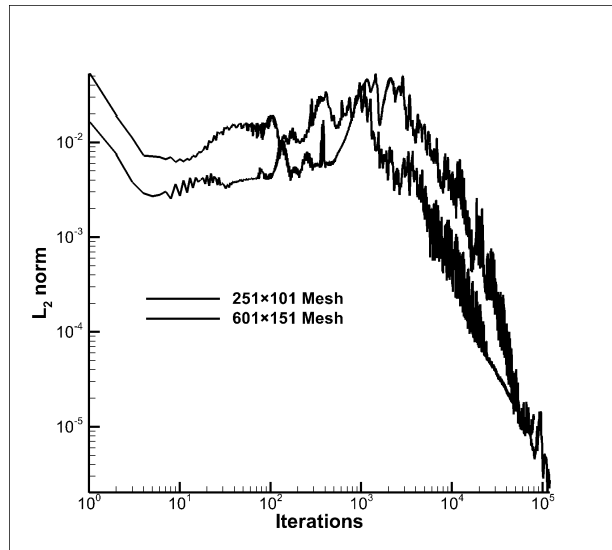


Figure 6: The convergence history of L_2 Norm relative error for the NASA SC(2)-1010 CFJ airfoil cases.

III.B. CFJ Constant Parameters and Freestream Conditions

The transonic airfoils, NASA SC(2)-1010 and NASA SC(2)-0714, maintain suction surface translation (SST) of 0.05%. Suction surface translation is a parameter that affects aerodynamic performance, and describes the translation of the suction surface toward the meanline in terms of percentage of chord length. These values are found to be the most efficient at cruise of the tested cases. The RAE-2822 airfoil has a SST of 0.1%, based on the transonic results of Liu et al.² SST variation is not explored in this paper, but may be considered for further study. The suction slot width, orientation and location are also maintained based on the best performing results of Liu et al.² Free-stream values for take-off condition, $M=0.1$ and $Re = 8.9 \times 10^5$ are used in this study. Similarly, for cruise condition, $M = 0.701$ and $Re = 6 \times 10^6$, based on the validation NASA SC(2)-1010 and NASA SC(2)-0714 airfoils. The cruise condition for RAE-2822 is $M=0.729$, based on the validation efforts of Liu.² As mentioned earlier, the mesh for CFD of each airfoil is based on the validated original airfoil. They are the more refined 601×151 mesh size.

III.C. CFJ Injection Slot Size and Location Study

For each airfoil, simulating a low-speed take-off condition involves changing not only the angle of attack, but the injection location and width for each case. Injection location is a percentage of chord and varies from 0.5% to 3%. This range is taken from previous studies at cruise, as well as observation of best take-off conditions. Injection width is similarly valued and ranges from 0.1% to 0.6%. Since the SST is fixed, some manual shaping of the suction surface is required to blend the injection slot with the rest of the airfoil. An ideal solution is a configuration that performs well at both takeoff and cruise.

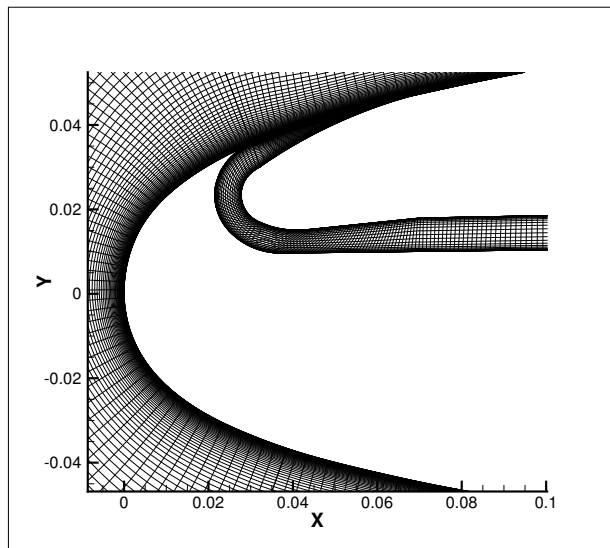


Figure 7: Mesh Example of Injection Location 3%, Injection Width 0.6% at $\alpha = 0^\circ$.

This is an example of the leading edge of the NASA SC(2)-0714 airfoil. The injection location is at 3% of the chord, while the injection slot thickness is 0.6%. The SST is 0.05% which makes it difficult to discern from this image alone.

III.D. NASA SC(2)-0714 Low-Speed

The NASA SC(2)-0714 airfoil is the thickest of the group studied. It has a more blunt nose, a larger radius at the leading edge. The flow can turn more gradually over the radius of the airfoil nose, which gives it an advantage at higher angles of attack. By placing the injection slot at the chord location of 3% and an injection width of 0.1%, the maximum lift coefficient is found to be 9.18. As defined earlier, the traditional C_{Lmax} for NASA SC(2)-0714 is 7.16, based on potential flow. This value is lower than the prospective lift coefficient for a CFJ airfoil according to Yang et al.³

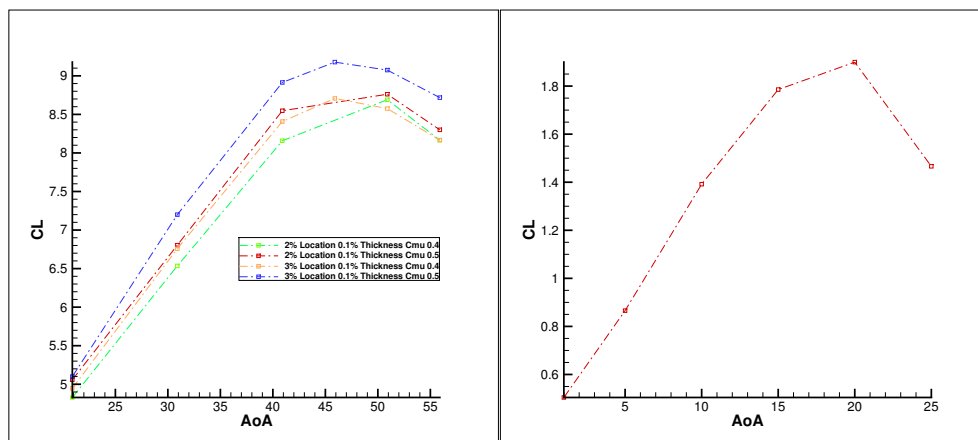


Figure 8: (A) C_L at location 2% and 3% with injection width 0.1% (B) Baseline Airfoil

The most noticeable characteristic of this CFJ configuration for NASA SC(2)-0714, which provides the highest lift coefficient of the tested cases, is that the injection jet velocity is supersonic. The nozzle works as a converging-diverging duct. Interestingly, by placing the injection slot closer to the leading edge to reduce separation, the lift coefficient decreases. It is possible that the leading edge separation creates a larger virtual leading edge radius, which ultimately affects lift.

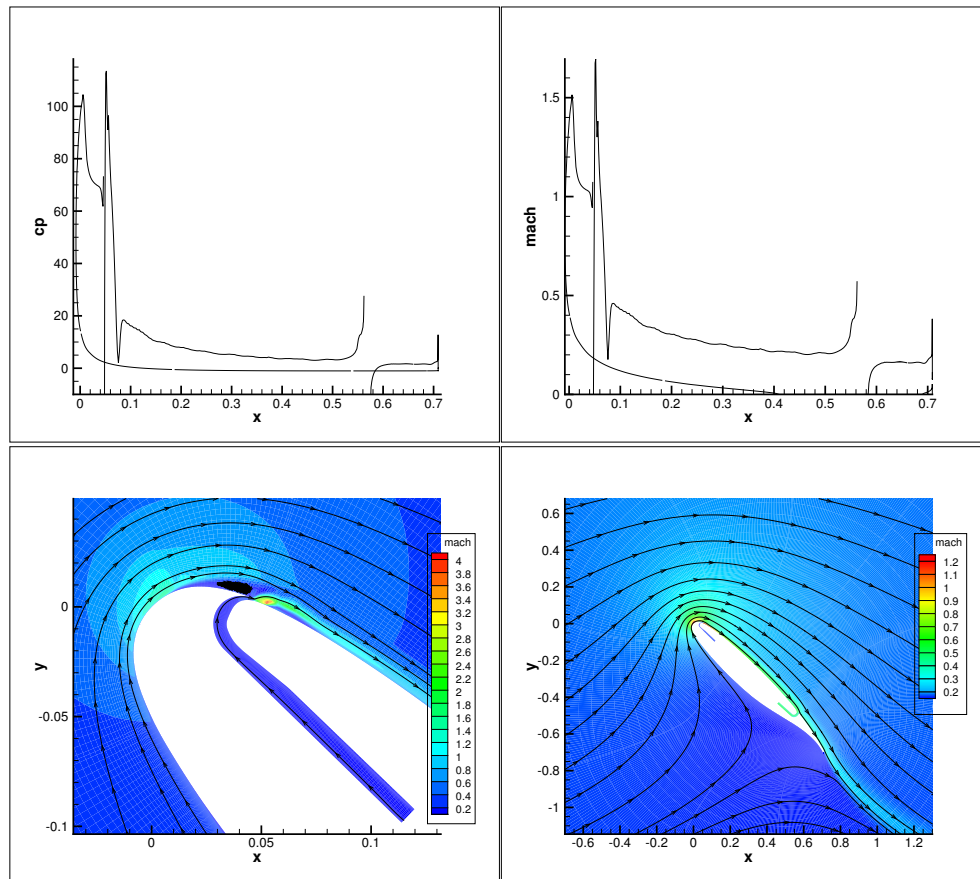


Figure 9: 45° angle of attack. $C_{\mu} = 0.5$. Injection Location 3%. Injection Width 0.1%

Another characteristic of varying C_{μ} is the ability to increase C_L given the same angle of attack. Previous studies show that the power requirement to allow the pressure ratio between injection and suction decrease as angle of attack increases due to the reduced static pressure at the injection location.³ This remains true for the regime where there is an attached boundary layer, but as seen in the close-up of the injection slot at 45° angle of attack, higher angles of attack cause a deterioration in boundary layer. This results in an increase in static pressure which increases pressure ratio and power requirements.

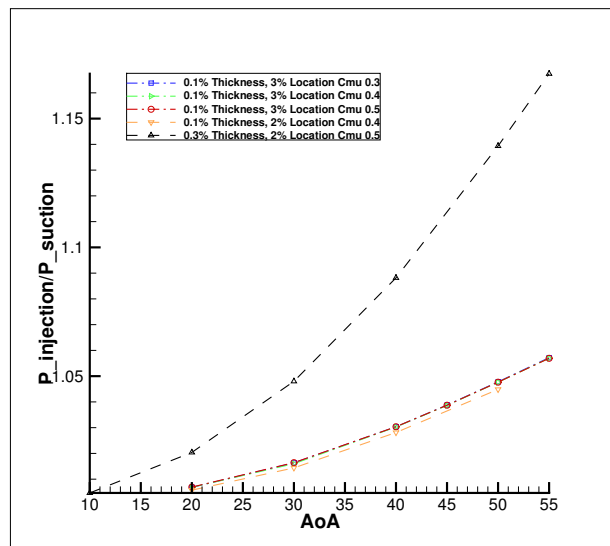


Figure 10: Pressure ratio

As mentioned, moving the the injection location to 2% in an attempt to reduce leading edge separation

and increase the possible angle of attack only serves to decrease the lift coefficient for this specific airfoil. Application to the other two airfoils in this study will determine whether this is true for other supercritical airfoils, or simply a product of geometric configuration.

Furthermore, while the larger radius of the airfoil nose helps maintain attached flow over the suction surface at higher angles of attack, as the injection jet location approaches the leading edge, the jet effect seems to oppose lift. This is simply due to geometry and the momentum of the jet itself. At an injection location of 0.5% and an injection width of 0.1%, the velocity of the jet is very high, but lift coefficient is reduced.

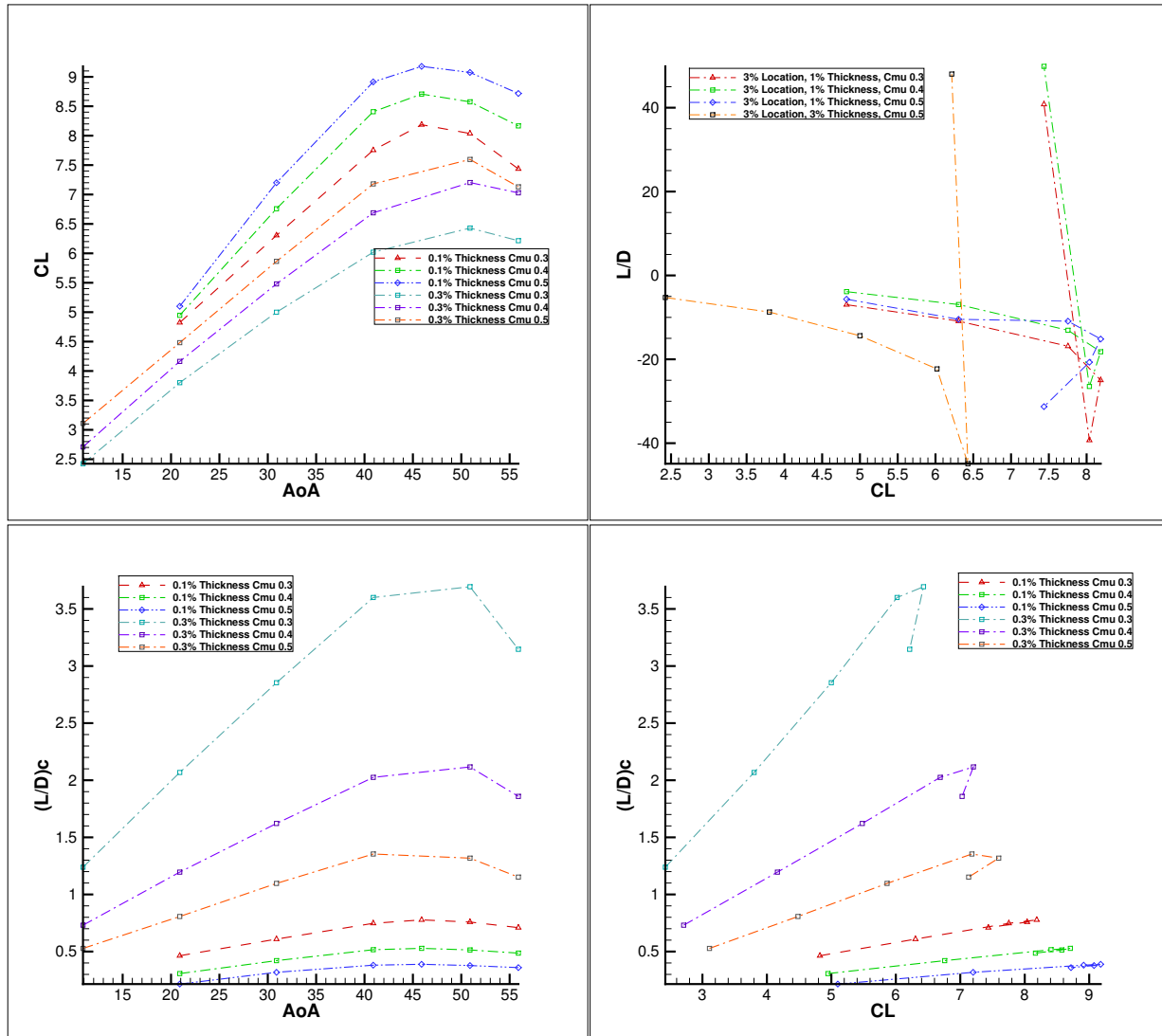


Figure 11: $(L/D)_c$ of NASA SC(2)-0714 Injection Location 3%, Thickness 0.1%-0.3%

With the injection location at 3%, the highest lift coefficient is achieved of the configurations tested. The small injection thickness means a very high jet velocity. High jet velocity decreases static pressure on the suction surface, which increases the lift coefficient. It also helps energize the boundary layer, causing better flow attachment over the rest of the suction surface. A disadvantage is higher power usage. Increasing the injection slot size reduces power usage but also decreases lift. The lift coefficient appears to be limited by how much energy can be injected into the flow. As one can see the $(L/D)_c$ value increases with larger injection thickness. When compared to the traditional (L/D) value, the jet actually produces thrust at lower angles of attack.

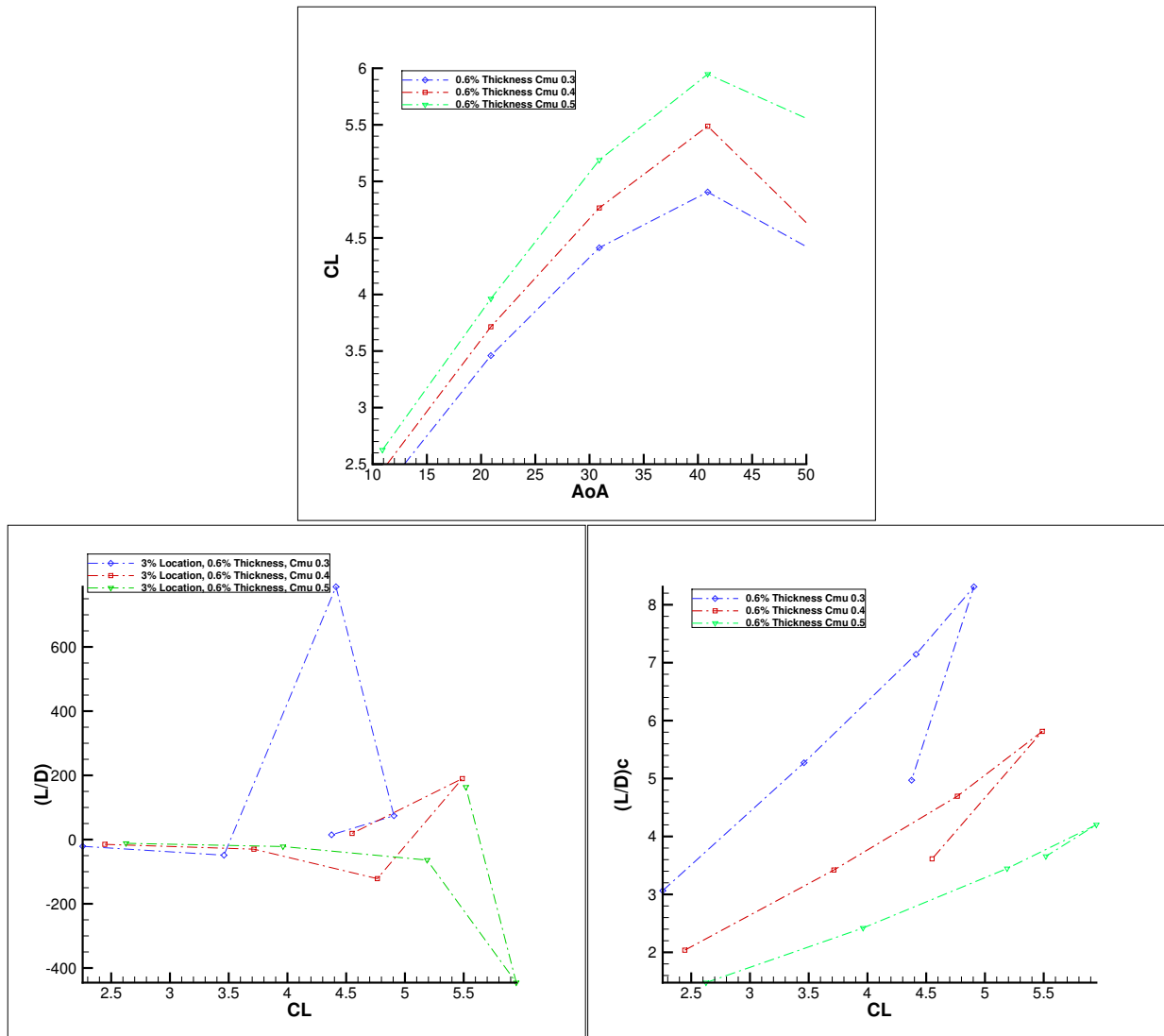


Figure 12: C_L and $(L/D)_c$ of NASA SC(2)-0714 Injection Location 3%, Thickness 0.6%

Using a larger injection thickness at 3% location gives a high C_L value, although lower than peak. The power consumption is significantly less, as $(L/D)_c$ is several times higher than that of smaller injection thickness. At higher C_μ values, the CFJ airfoil is producing thrust as seen above.

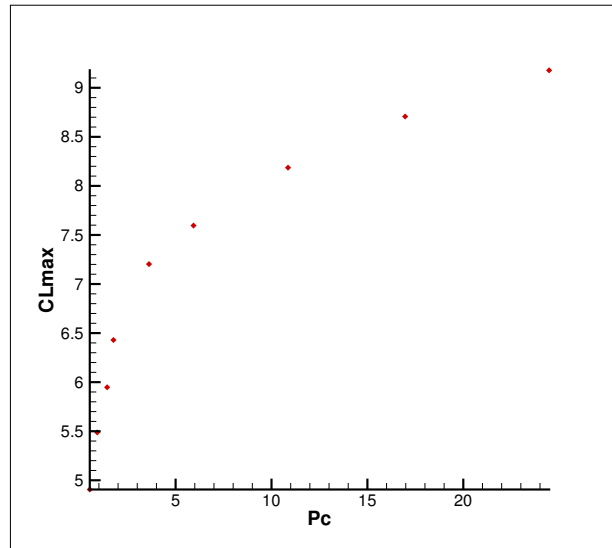


Figure 13: Maximum Lift Coefficient of Each Configuration v Power Coefficient

The maximum lift coefficient for each configuration as a function of power coefficient can be seen in the above figure. This includes different injection sizes and locations. The CFJ airfoil approaches a maximum lift coefficient of over 9. The power required to increase the lift of the airfoil has diminishing returns with increasing value. This plot shows the power coefficient and maximum lift coefficient follow a curve regardless of injection location and slot thickness. The maximum lift coefficient seems to follow the same logarithmic curve, and is a topic ripe for further study.

III.E. RAE-2822 Low-Speed

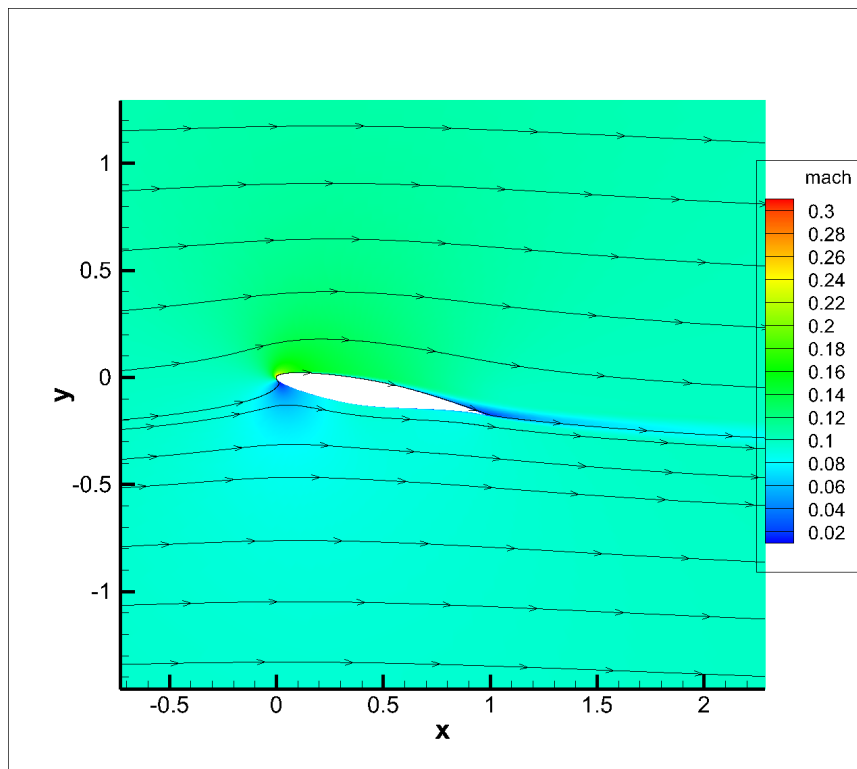


Figure 14: 10° Angle of Attack Baseline Airfoil

The RAE-2822 super-critical airfoil study keeps a 0.1% SST fixed, which provides high performance at cruise according to Liu et al.² Using similar injection width variation as NASA SC(2)-0714, going from

0.1% to 0.6%, allows 0.1% width to match the SST, which makes mesh generation simpler. The RAE-2822 airfoil has a much sharper radius at the leading edge. This means the flow over the airfoil has to turn more sharply at higher angles of attack, increasing the probability of leading edge separation. The following figure is the baseline airfoil stalling at 15° angle of attack. In contrast by applying CFJ to the airfoil, it is able to achieve 40° . For the baseline airfoil at 10° , the coefficient of lift is only 1.15.

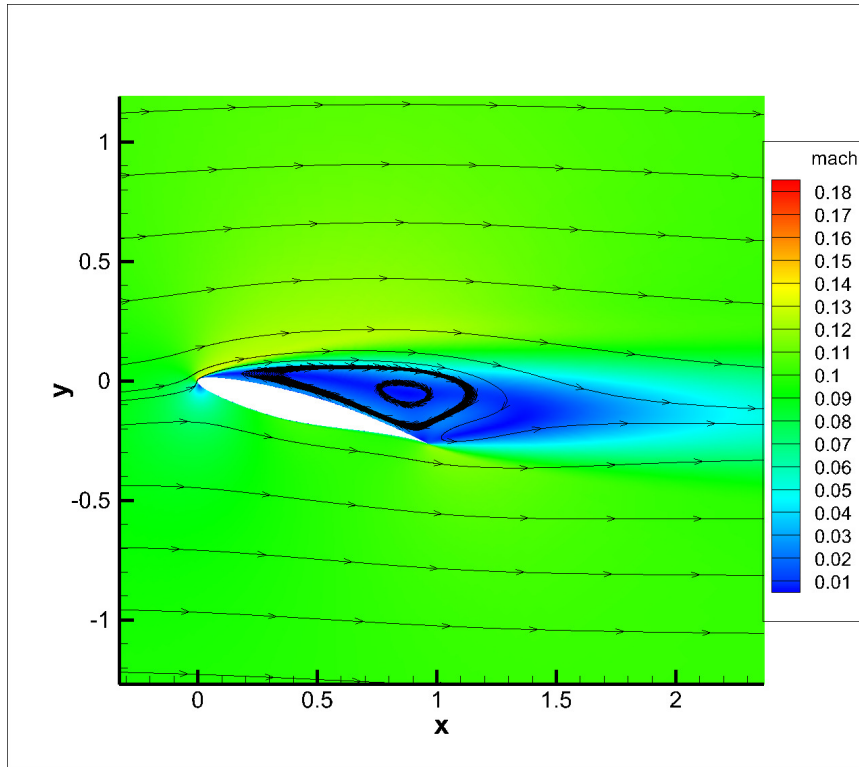


Figure 15: 15° Angle of Attack Baseline Airfoil

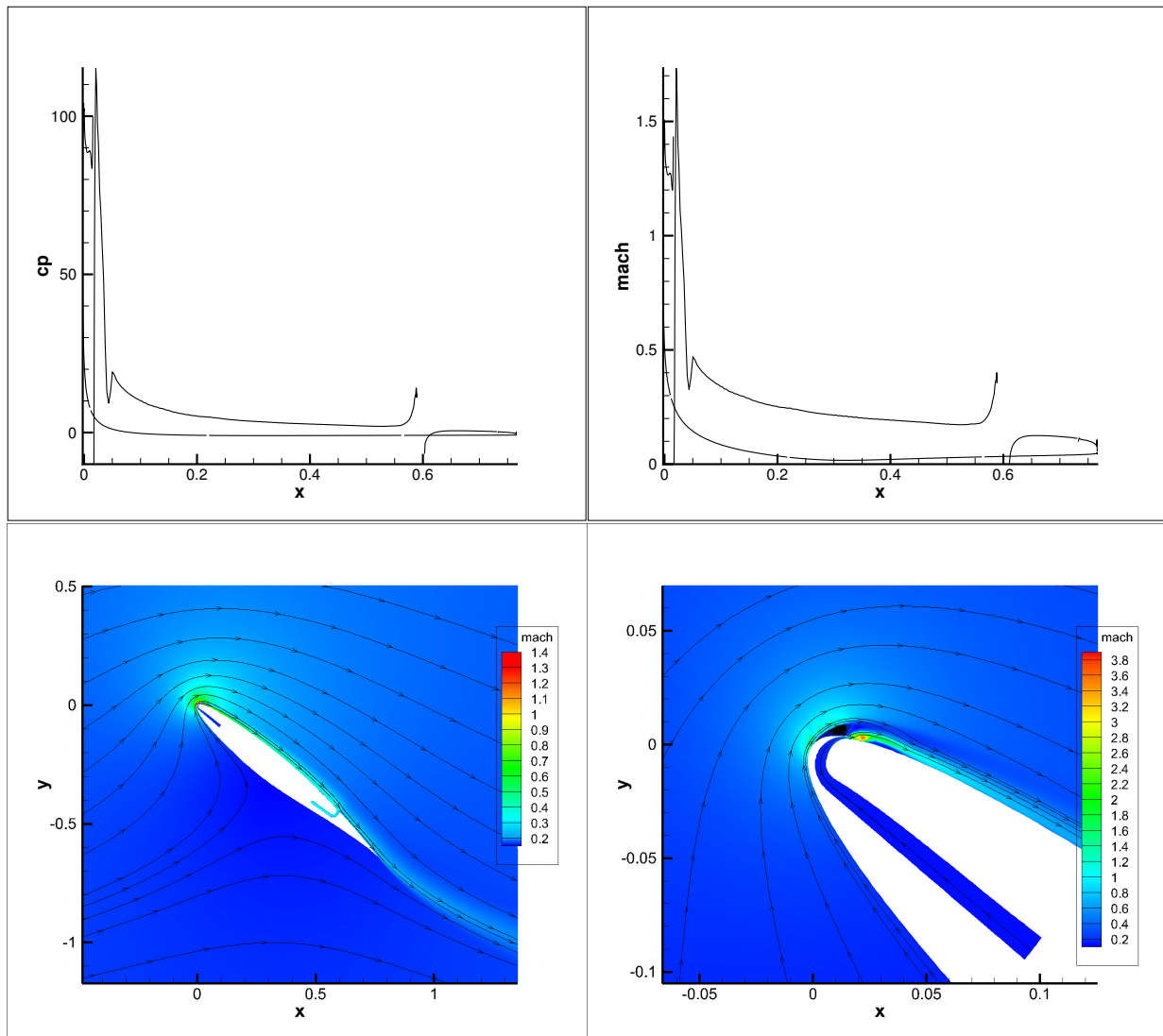


Figure 16: 40° Angle of Attack with $C_l=5.4$. 1% Injection Location. 0.1% Injection Width

Due to the geometry difference between NASA SC(2)-0714 and RAE-2822 airfoils, it is not able to achieve super-lift above the potential flow limit, C_{Lmax} of 7.04. As one can see the flow accelerates to sonic condition as it turns over the nose of the airfoil. The smaller radius at the leading edge makes the flow turning sharper. The leading edge separation is a difficulty that needs to be overcome with supercritical airfoils at high angles of attack, although the CFJ airfoil seems to use it to its advantage. The smaller leading edge radius RAE-2822 compared to NASA SC(2)-0714 means the flow has to make a sharper turn and the injection slot needs to be placed closer to the leading edge. The injection location is placed as far forward as 0.5%. Internal ducting also needs to be considered, as internal space constraints complicates this as well. The results show that the most forward location is not the best, and the leading edge separation, once again, allows the streamlines to follow a blunter virtual leading edge. Another interesting side-effect of the CFJ airfoil at high C_μ values is the jet producing thrust. The Mach contour plot at high C_μ shows the CFJ filling the wake velocity deficit, with a high-velocity stream of air flowing past the trailing edge of the airfoil.

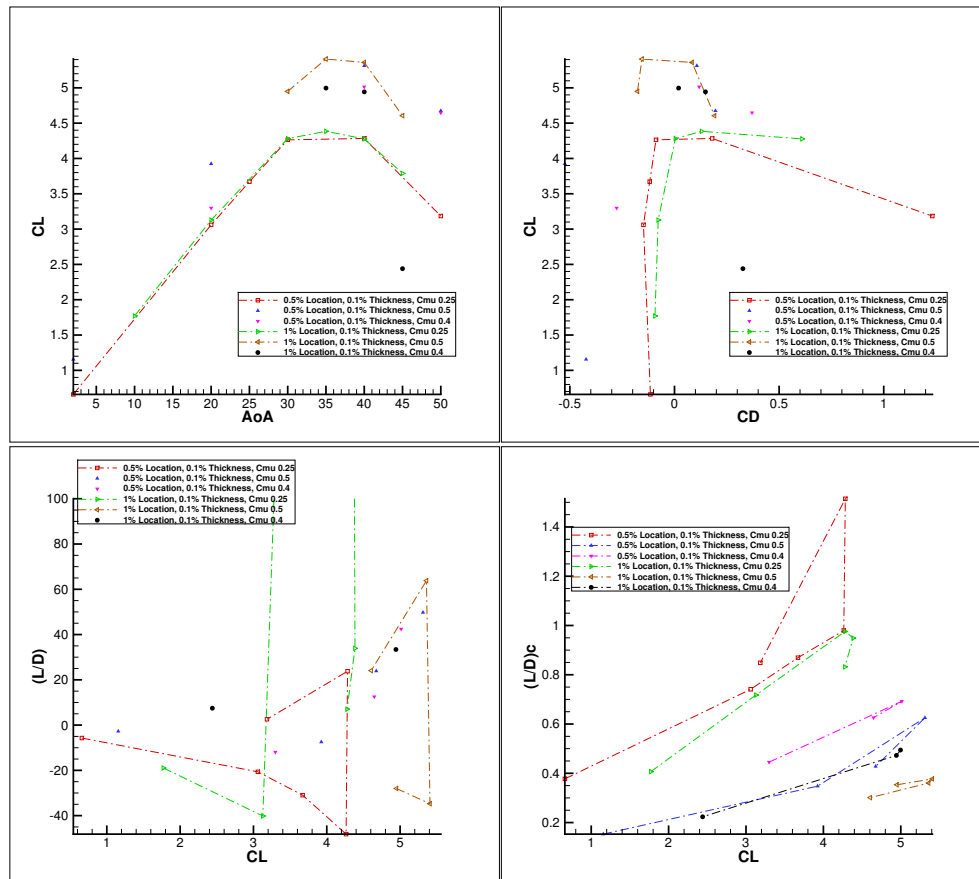


Figure 17: 0.5%-1% Injection Location. 0.1% Injection Width

The lift results from 1% and 0.5% injection location are relatively similar. This seems like an obvious conclusion because the 0.5% difference along the chord is a small value, though it is significant in that it does affect drag and efficiency. The drag values differ somewhat which causes the denominator in both C_L/C_D and $(L/D)_c$ to approach zero at certain points tested. The point farther from the leading edge provides less drag, even thrust at small slot widths and high C_μ values.

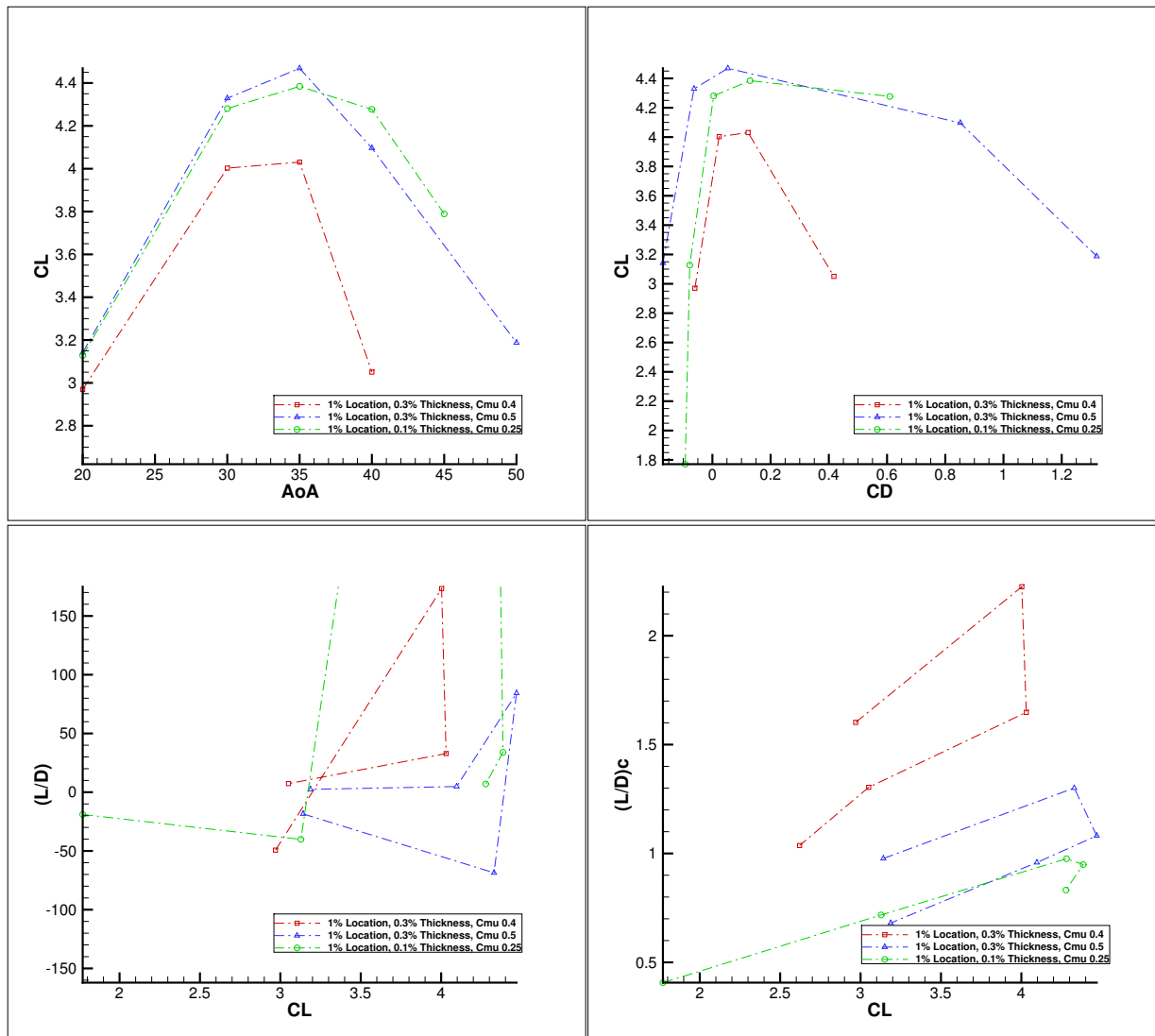


Figure 18: 1% Injection Location. 0.1%-0.3% Injection Width

At 1% injection location, the CFJ has a similar power coefficient at 0.1% injection width at C_{μ} of 0.25 as at 0.3% injection width at C_{μ} of 0.5. The C_L values are similar as seen in the figure above. What differs is the drag values, which is attributed to the velocity of the jet. This, in turn, provides a higher $(L/D)_c$ value.

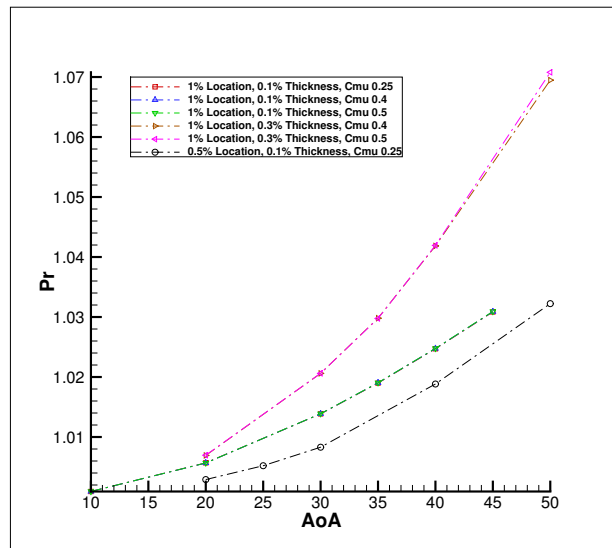
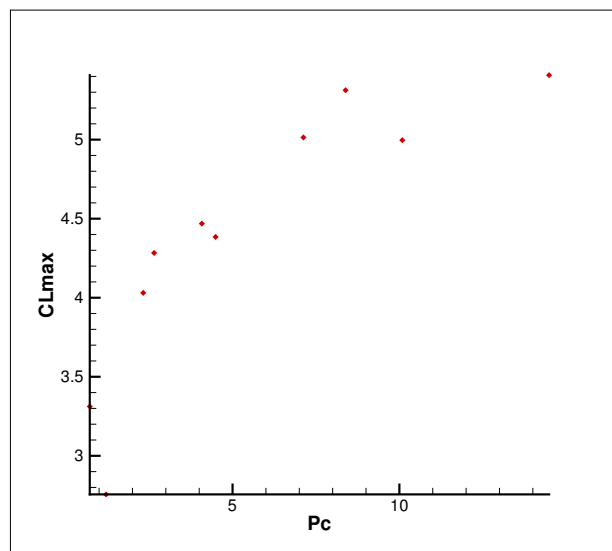


Figure 19: RAE-2822 CFJ Pressure Ratio

The pressure ratio for the CFJ at various injection location and thicknesses show several things. First of all, the pressure ratio is largest farther from the leading edge of the airfoil. This may be due to increased flow separation. The pressure ratio also increases the larger the injection slot. The pressure ratio values are identical at different C_μ values given the same geometry.

Figure 20: RAE-2822 P_c v C_L

The maximum lift coefficient for each configuration plotted against the power coefficient exposes the same trend as NASA SC(2)-0714. The lift coefficient increases to a certain value, all the while the power coefficient reflects diminishing returns. A comparison with NASA SC(2)-0714 shows that the lift coefficients are different given the same power coefficient because of different surface geometry. The smaller radius of the leading edge may correlate to the difference in C_{Lmax} and, once again, is a candidate for further study.

III.F. NASA SC(2)-1010 Low-Speed

The NASA SC(2)-1010 airfoil has a less sharp leading edge than the RAE-2822, but is still slender for efficient performance at cruise. It is the thinnest of the group at 10% thickness. The baseline airfoil, with freestream $M=0.1$, stalls at 20° . This not very surprising, as transonic airfoils tend to be very efficient at cruise, but are not ideal over a large range of angles of attack.

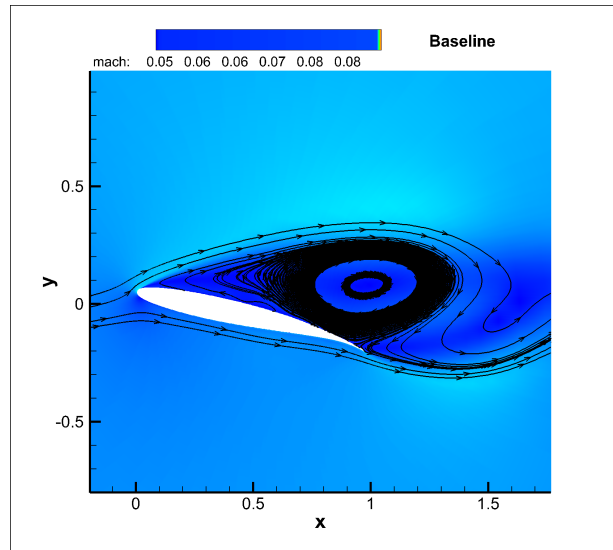


Figure 21: Mach contours of NASA SC(2)-1010 baseline airfoil at $\alpha = 12^\circ$.

Using the same methodology as varying the injection location and width of both NASA SC(2)-0714 and RAE-2822, the largest coefficient of lift is found and studied. The baseline airfoil stalls as early as 12° angle of attack. Applying CFJ to the airfoil gives a peak C_L of 5.9 at 35.5° .

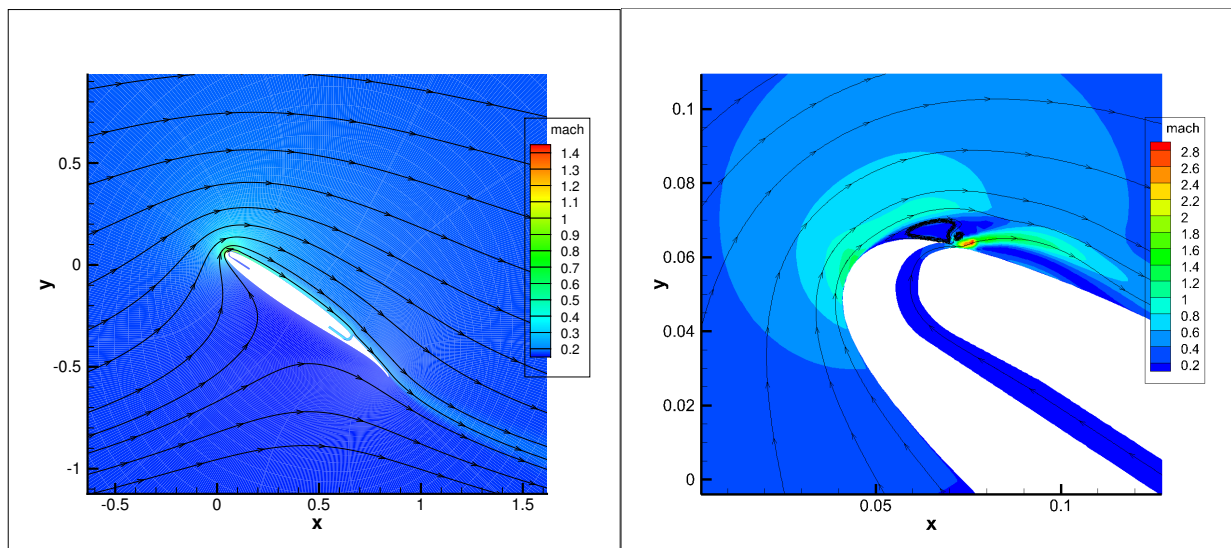


Figure 22: NASA SC(2)-1010 Injection Location 2%, Thickness 0.1%, $C_L = 5.9$, $C_\mu = 0.5$

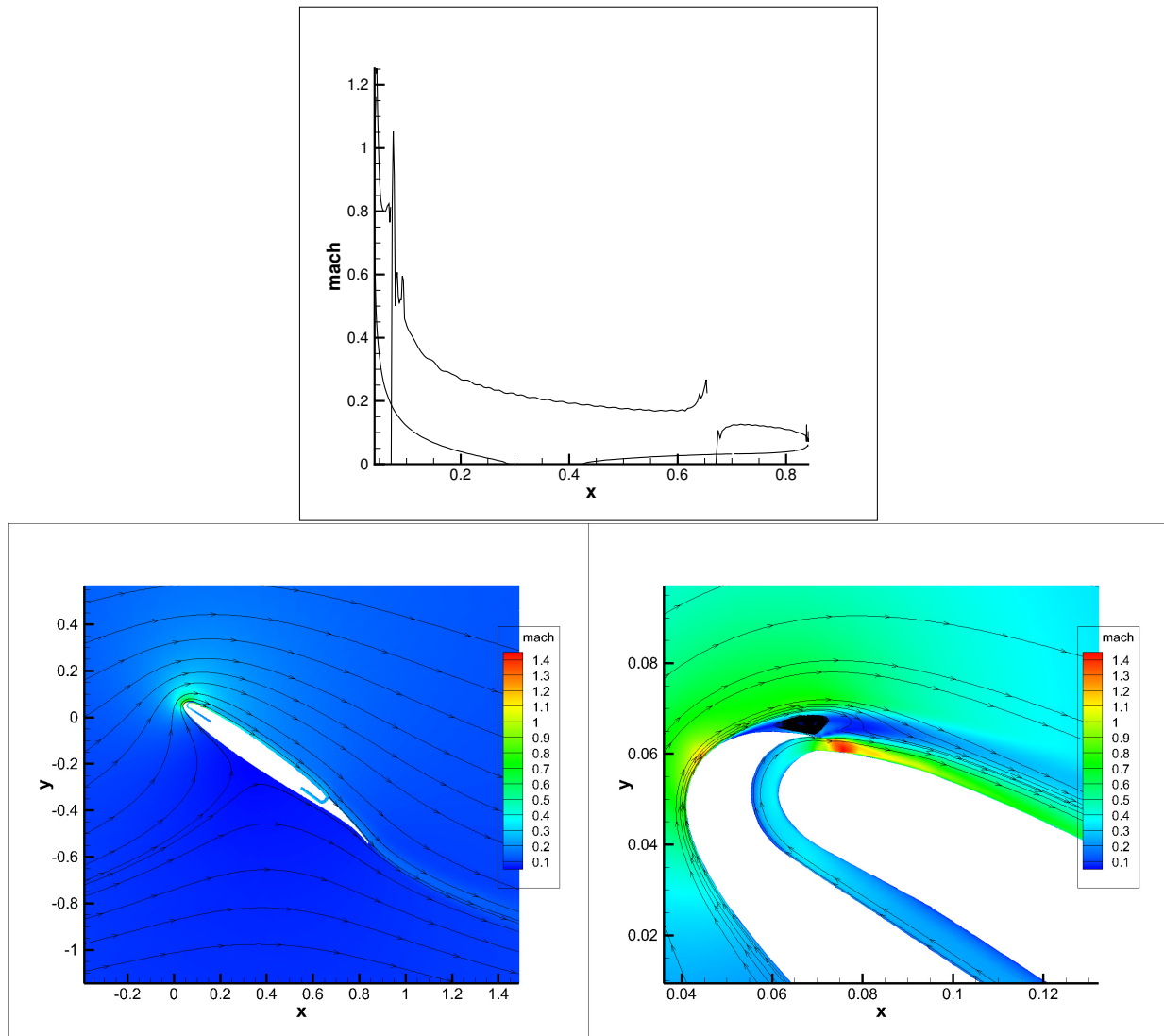


Figure 23: NASA SC(2)-1010 Injection Location 2%, Thickness 0.3%, $C_L = 5.24$, $C_\mu = 0.5$

By increasing the injection size, the jet more nicely follows the suction surface of the airfoil, decreasing shock strength leaving the slot, while still achieving very high lift. The power coefficient also decreases significantly between 0.1% injection thickness and 0.3% injection thickness. The latter case has a value of 2.95, while the former is significantly higher at 11.76. In both cases there is some leading edge separation, and while boundary layer degradation would be an issue for the baseline airfoil, the injection jet energizes the flow. By moving the injection slot forward to 1%, the CFJ eliminates some leading edge separation, but the C_L sees no benefit at $C_\mu=0.4$, and the numerical simulation becomes somewhat unstable at higher C_μ values. In the later transonic study, the 2% location is more efficient than the 1% location, besting the efficiency of the baseline airfoil. At 0.6% thickness and 1% location, the CFJ airfoil has very little leading edge separation, and a small power coefficient of 0.956, but results in lower lift values.

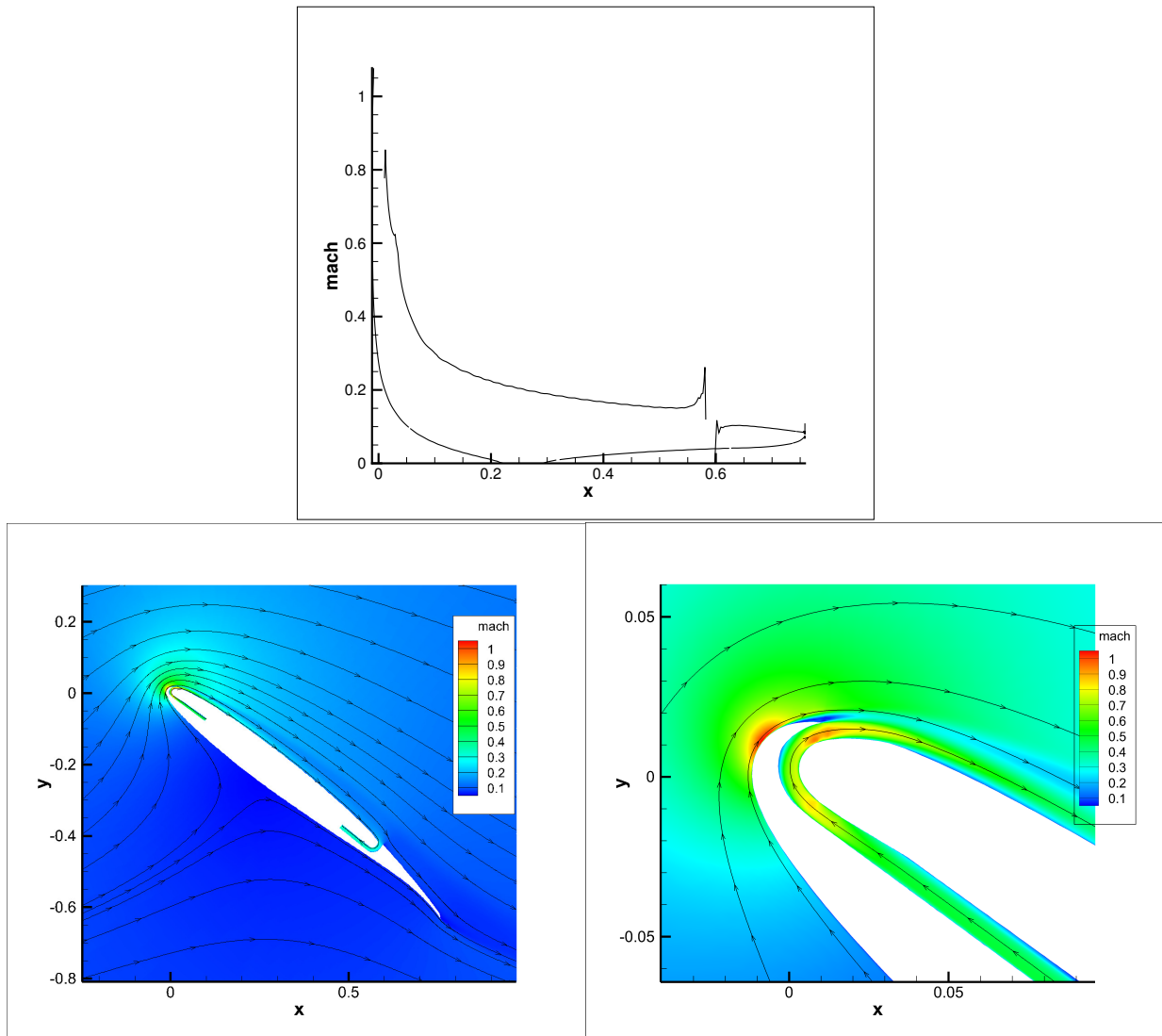


Figure 24: NASA SC(2)-1010 Injection Location 1%, Thickness 0.6%, $C_L = 4.47$, $C_\mu = 0.5$

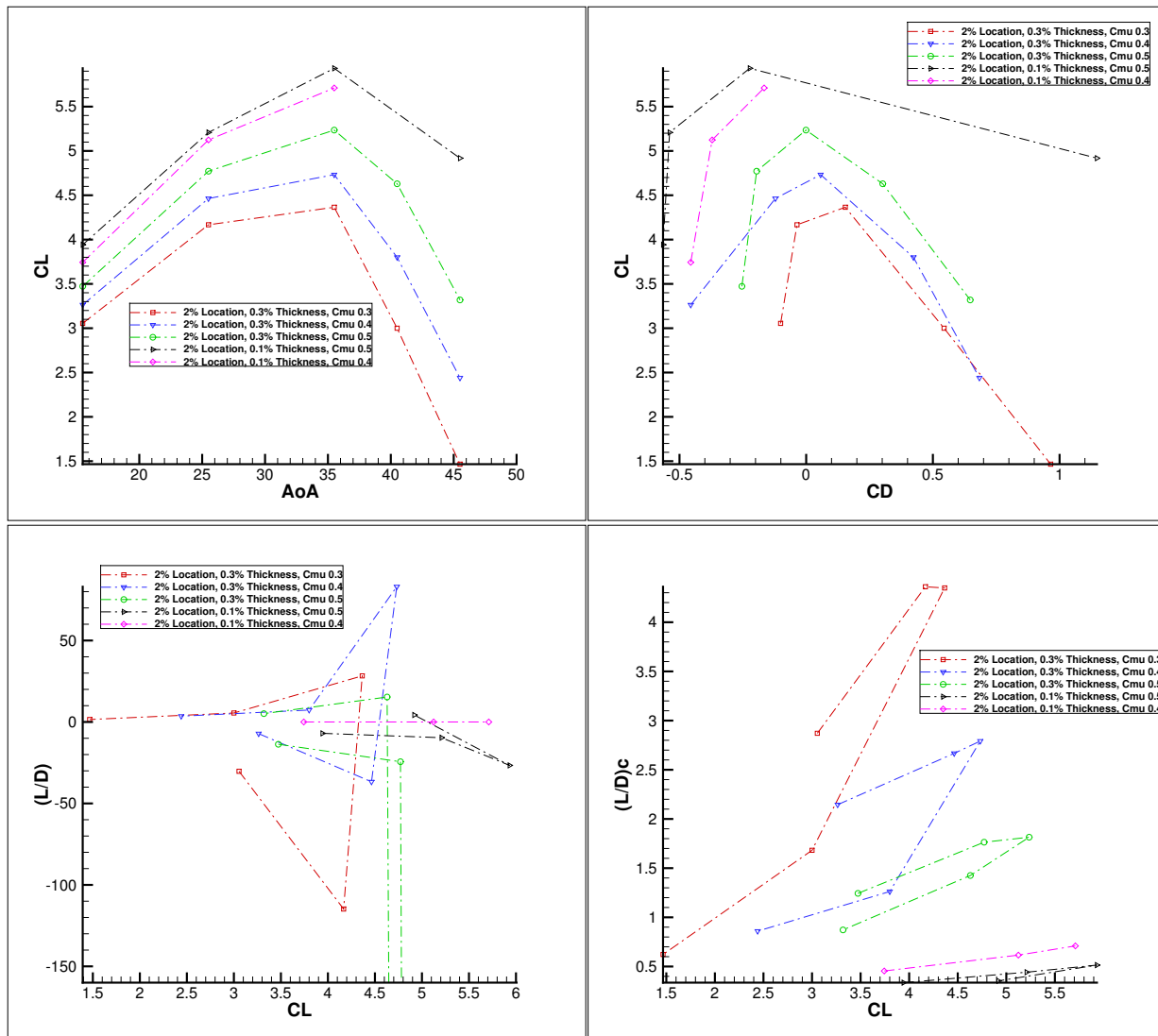


Figure 25: NASA SC(2)-1010 Injection Location 2%, Thickness 0.1% and Thickness 0.3%

This airfoil shows higher lift performance than RAE-2822 while being thinner and having less drag. The drag coefficient is negative at higher C_{μ} values, which indicates the injection jet is actually producing thrust. The value of L/D is hard to compare to the baseline airfoil. Since the jet produces thrust, the drag may actually approach zero. This means the ratio approaches infinity as shown above. The corrected ratio, $(L/D)_c$ shows that NASA SC(2)-1010 is actually more efficient at a given C_L than NASA SC(2)-0714 even though the peak lift coefficient is smaller. This happens at 2% location, which, based on transonic CFJ studies of the same airfoil is the best location at cruise. The power coefficient for a lift coefficient of 4.4 at 0.3% injection thickness and $C_{\mu} = 0.3$ is $P_c = 0.85$. For the peak lift coefficient of 5.9 at 0.1% thickness and $C_{\mu} = 0.5$, $P_c = 11.8$. That is a very large difference for a 34% increase in lift. As with NASA SC(2)-0714 and RAE-2822, there is diminishing returns for power increase on lift coefficient.

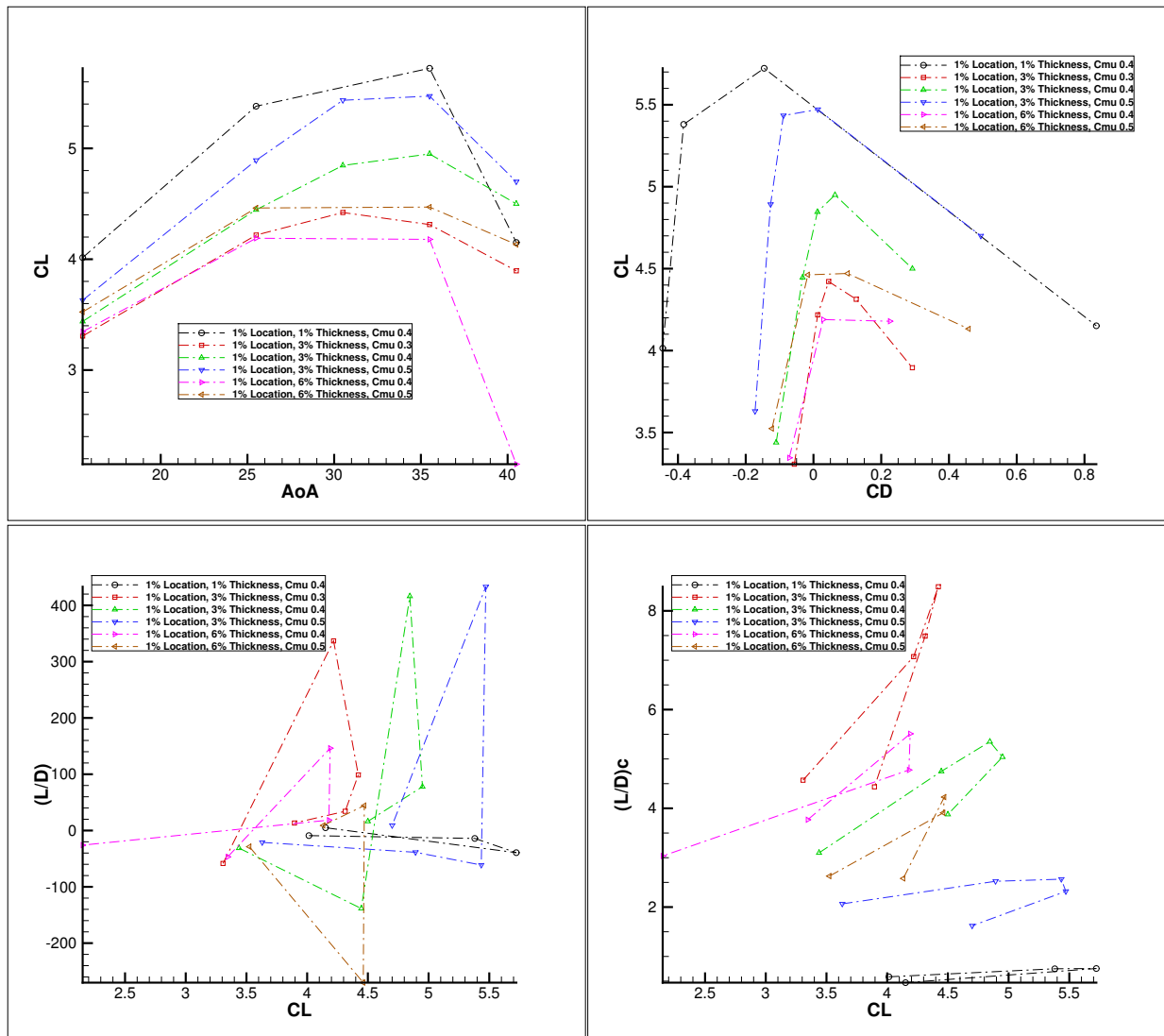


Figure 26: NASA SC(2)-1010 Injection Location 1%

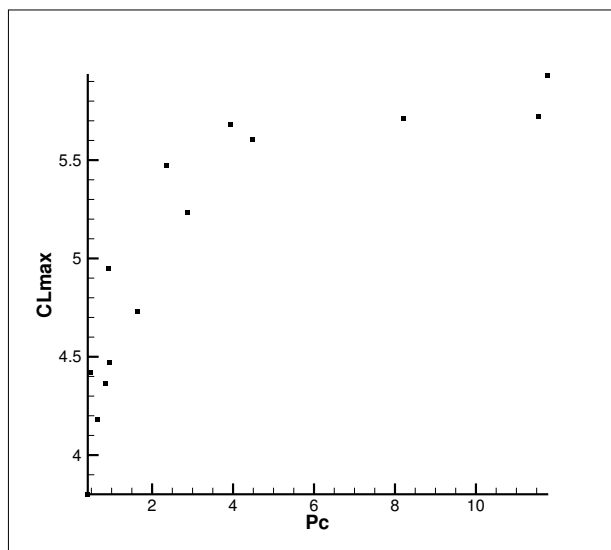


Figure 27: NASA SC(2)-1010 CL_{max} v P_c

III.G. Transonic CFJ Airfoil Study

III.H. NASA SC(2)-1010 at Mach 0.701

For the transonic CFJ airfoil study, configurations that provide good low-speed performance are tested at cruise. Suction surface translation (SST) of 0.05% is used with the injection slot size of 0.6% of the chord. A previous study by Liu et al.² showed that the value of SST plays a significant role in the aerodynamic performance of a CFJ airfoil at transonic conditions. The suction slot size, orientation and location have been kept in accordance with the best results obtained by Liu et al.² Free stream values, $M=0.701$ and $Re = 6 \times 10^6$ are used for this study.

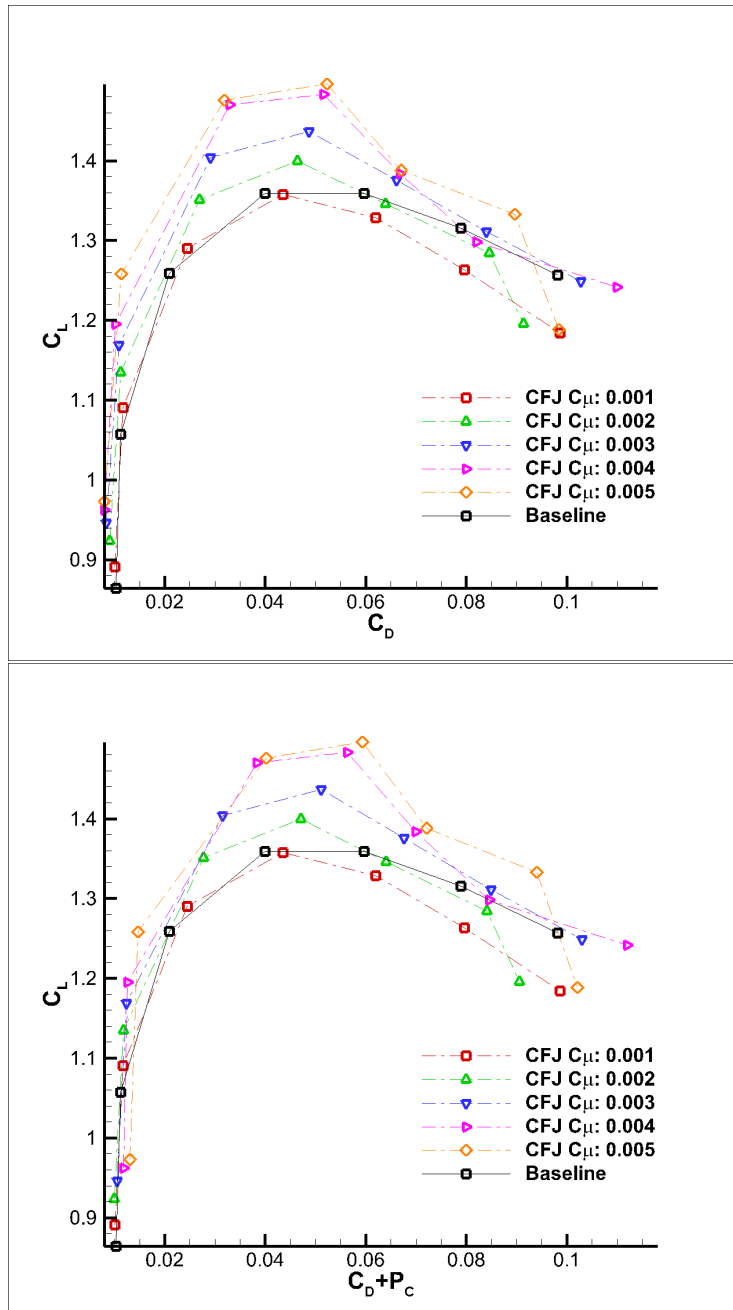


Figure 28: CFJ and baseline airfoil drag polar curves for angle of attack ranging from -2° to 4°

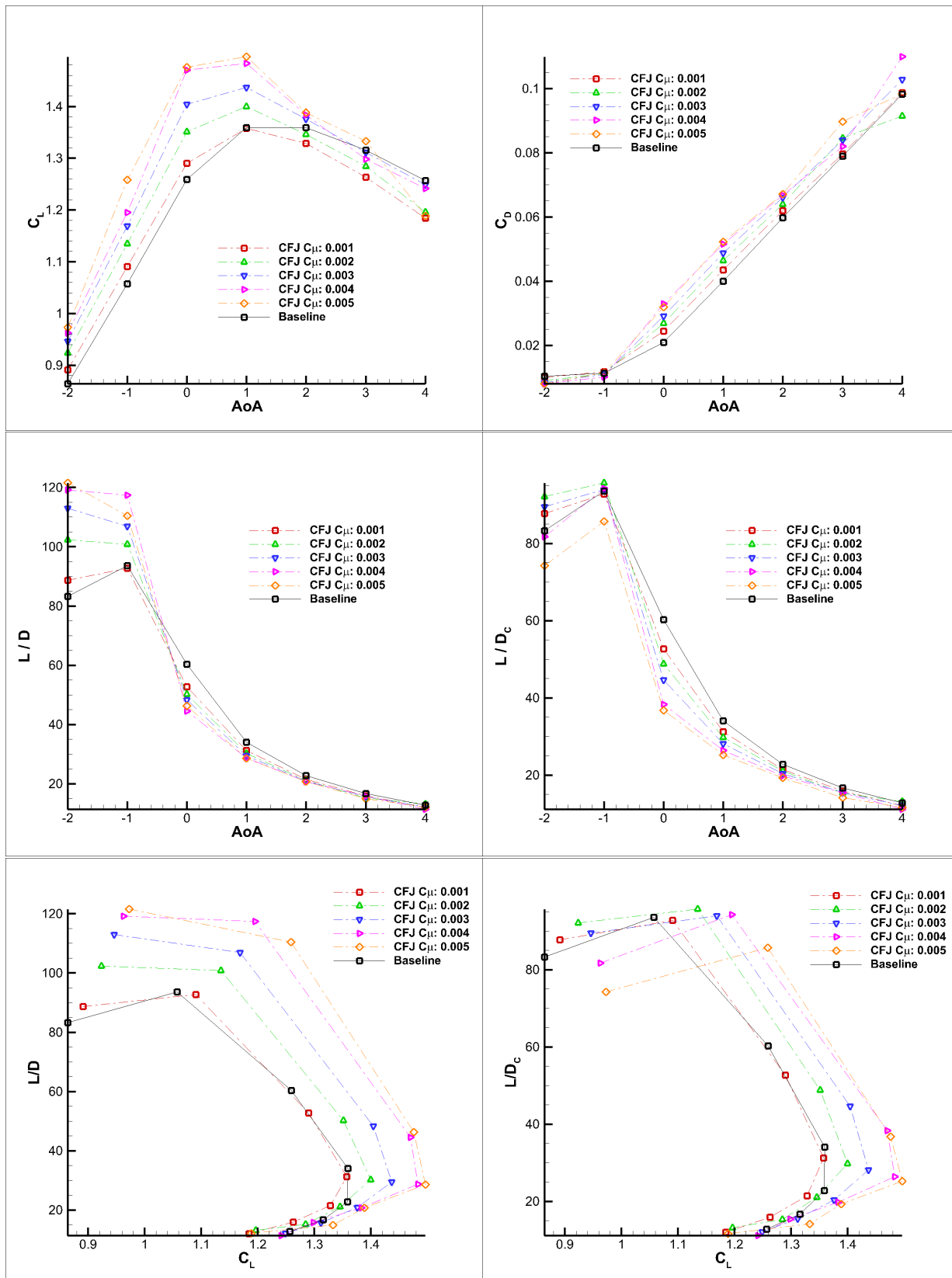
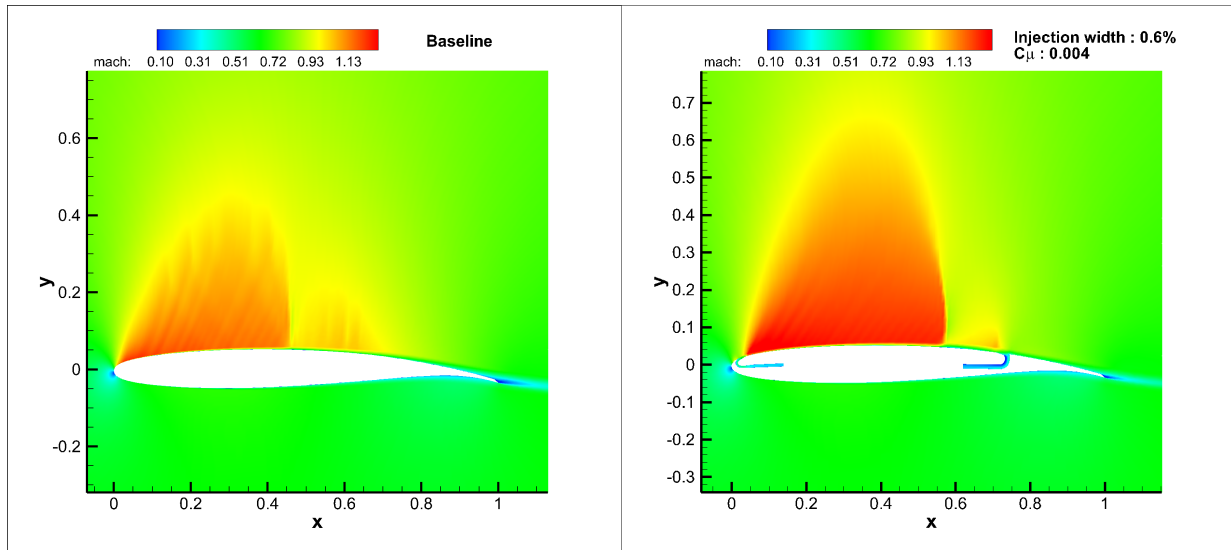
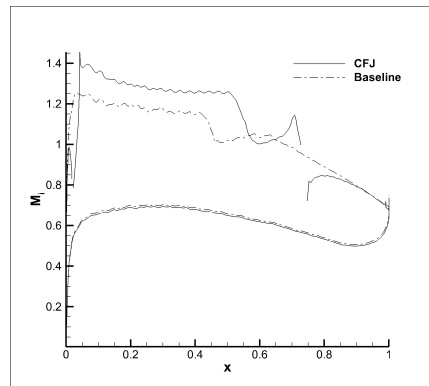


Figure 29: CFJ and baseline aerodynamic performance curve for angle of attack ranging from from -2° to 4°

Figure 30: Mach contours for baseline and CFJ airfoils at $\alpha = -1^\circ$ Figure 31: Isentropic Mach distribution comparison between baseline and CFJ airfoils at $\alpha = -1^\circ$ Table 2: CFJ airfoil aerodynamic coefficients comparison between baseline and CFJ airfoils for different injection slot sizes at different C_μ and $\alpha = -1^\circ$.

Inj. Slot Width	C_μ	C_L	C_D	P_C	$(\frac{L}{D})$	$(\frac{L}{D})_c$
Baseline	0.000	1.057	0.0113	0.000	93.560	93.560
0.3%	0.004	1.174	0.0094	0.0023	124.898	100.344
0.06%	0.001	1.062	0.0108	0.0006	107.692	101.514

At cruise the NASA SC(2)-1010 airfoil is more efficient than the baseline airfoil with the injection location at 2%. Various injection sizes are more efficient than baseline. Based on the mach contours, the shock wave is pushed toward the trailing edge, improving on the supercritical airfoil design. The advantage of using this location and size means the same geometry can provide an advantage at cruise and at takeoff.

III.I. NASA SC(2)-0714 at Mach 0.701

Similarly for the NASA SC(2)-0714 CFJ airfoil, using the same injection location as the best low-speed performance, 3%; the configuration with 0.3% injection width was found to have superior cruise performance when compared to the baseline airfoil.

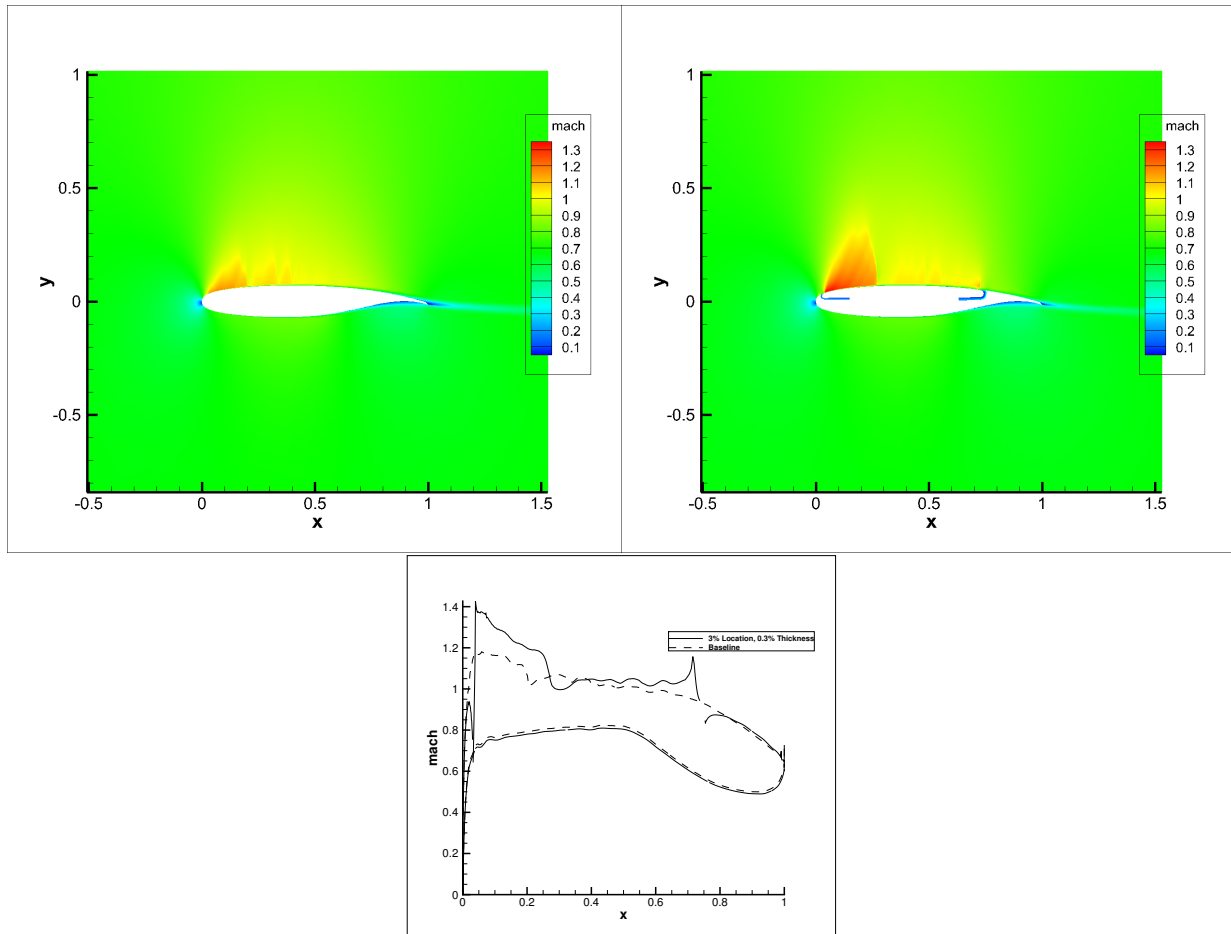


Figure 32: NASA SC(2)-0714 $M = 0.701$ at $\alpha = 1^\circ$ baseline and 3% Location, 0.3% Injection Width

The main shock is pushed further along the chord in the CFJ airfoil when compared to the baseline airfoil. The advantage of this configuration is it provides great takeoff performance and improves on the baseline airfoil at cruise.

Table 3: CFJ airfoil aerodynamic coefficients comparison between baseline and CFJ airfoil at $\alpha = 1^\circ$.

Inj. Slot Width	C_μ	C_L	C_D	P_C	$(\frac{L}{D})$	$(\frac{L}{D})_c$	$(\frac{C_L^2}{C_D})_c$
Baseline	0.000	0.723	0.0115	0.000	62.84	62.84	45.42
0.3%	0.003	0.829	0.00995	0.003	83.28	64.00	53.06

This particular configuration excels at both cruise and low-speed conditions. An even better configuration can most likely be found, and is a candidate for future study.

III.J. RAE-2822 at Mach 0.729

RAE-2822 is tested at Mach 0.729 as opposed to 0.701 of the other airfoils, due to basing the mesh and validation results off the work of Liu.² It has already been seen in previous publications that this airfoil outperforms the baseline airfoil at cruise when using the same CFJ configuration, but with the injection slot at 3% and 0.6% width. Testing the injection location much closer to the leading edge provides promising results, although less than optimal at cruise.

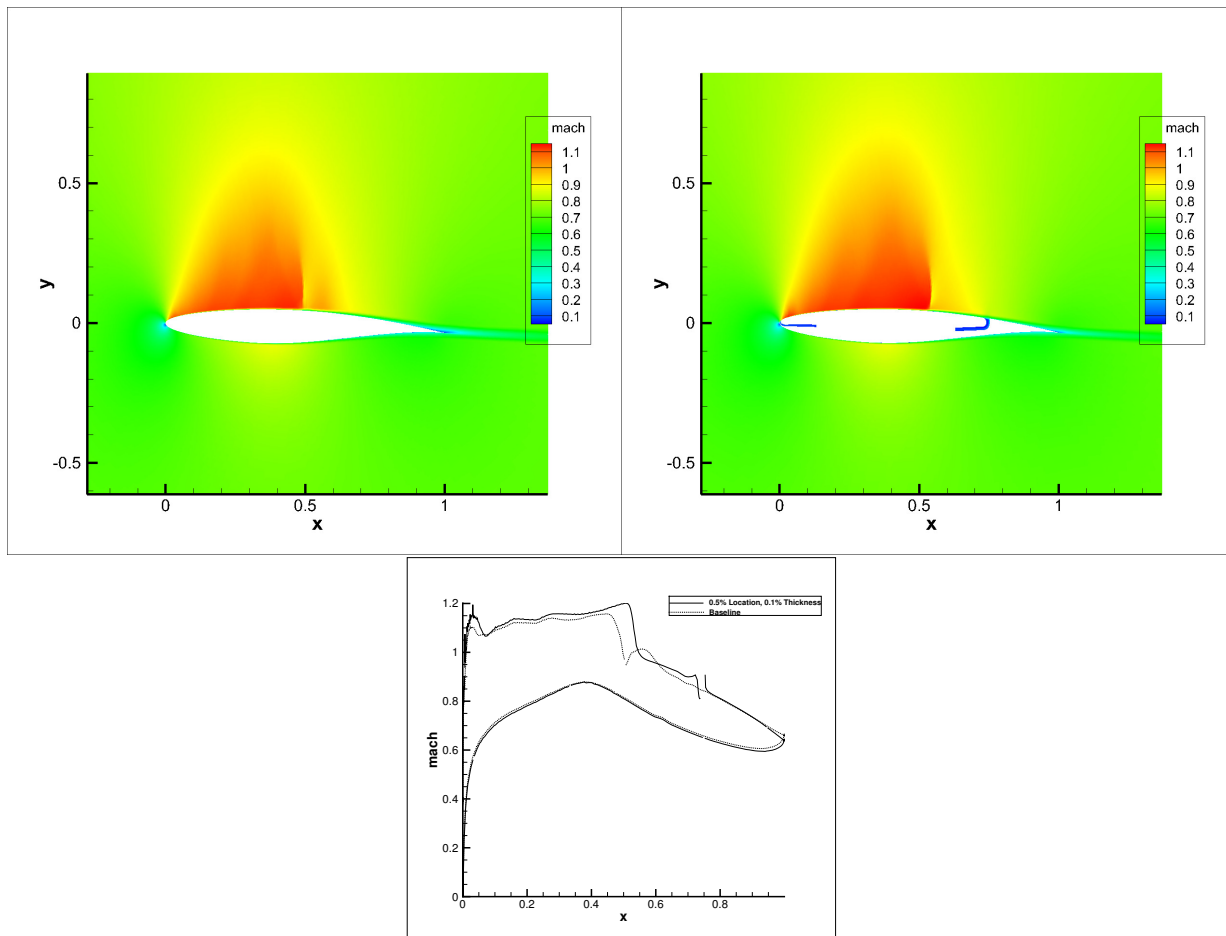
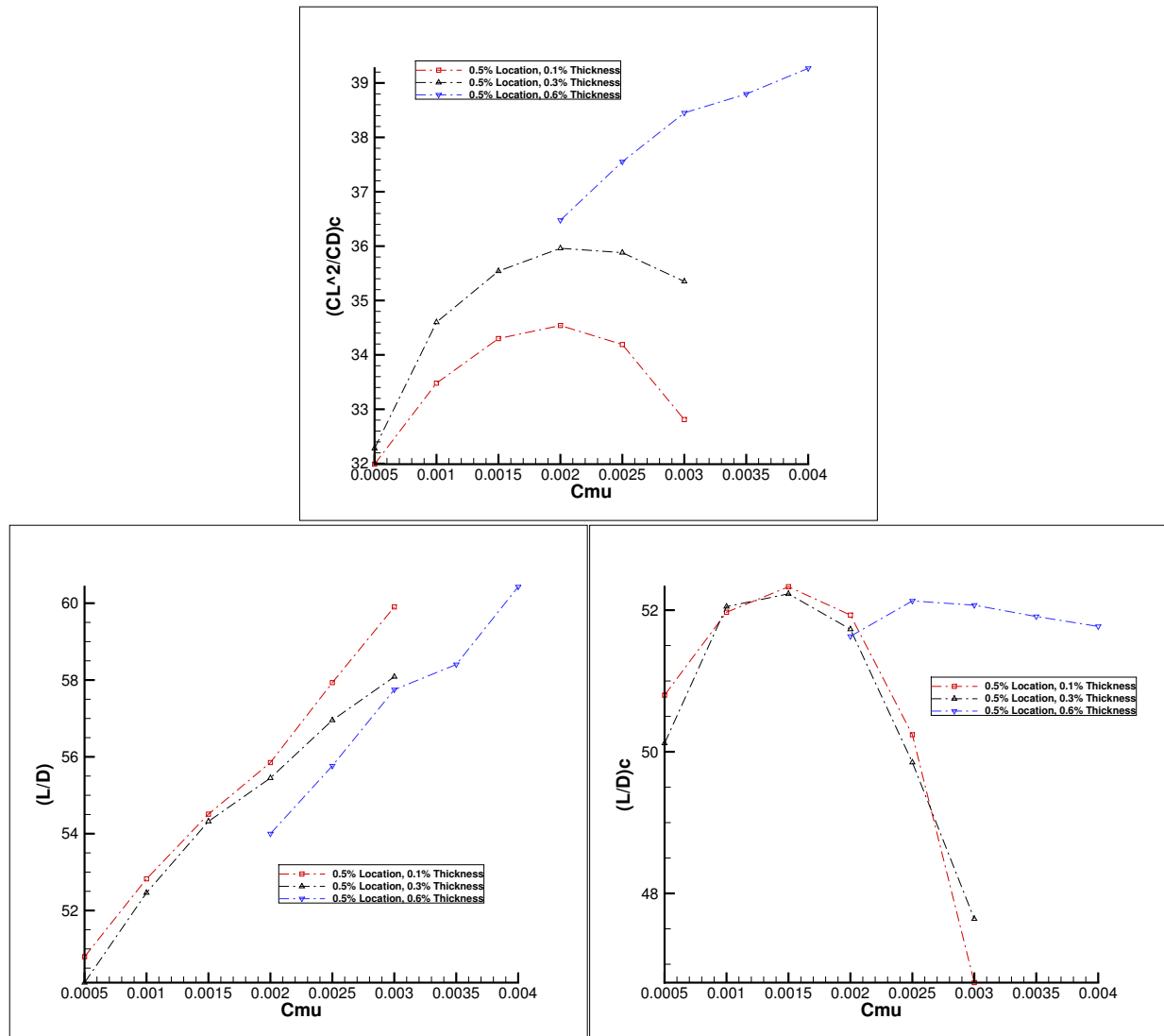


Figure 33: RAE-2822 $M = 0.729$ at $\alpha = 2^\circ$ baseline and 0.5% Location, 0.1% Slot Width

Figure 34: RAE-2822 $M = 0.729$ at $\alpha = 2^\circ$.Table 4: CFJ airfoil aerodynamic coefficients comparison between baseline and CFJ airfoils for different injection slot sizes at different C_{μ} and $\alpha = 2^\circ$.

Inj. Slot Width	C_{μ}	C_L	C_D	P_C	$(\frac{L}{D})$	$(\frac{L}{D})_c$	$(\frac{C_L^2}{C_D})_c$
Baseline	0.000	0.611	0.0123	0.000	49.68	49.68	30.35
0.1%	0.0015	0.656	0.0121	0.0005	54.51	52.33	34.15
0.3%	0.0015	0.680	0.0125	0.0005	54.32	52.23	35.57
0.6%	0.0025	0.720	0.0129	0.0009	55.77	52.13	37.57

The plot of corrected productivity coefficient is higher for all tested points than the baseline airfoil at 30.35. This reflects the ability to carry load over distance. The best point for productivity coefficient is different than that of the largest $(L/D)_c$ value. Even at this point, it exceeds the baseline value.

IV. Conclusion

The low-speed performance of CFJ supercritical airfoils prove to have superior lift coefficients when compared to the baseline performance. This provides an opportunity for high lift systems with no flaps to achieve ESTOL performance, while also giving an advantage at cruise. The CFJ-NASA SC(2)-0714 airfoil

at low speed is improved by more than doubling the stall angle of attack. The most important result is the increase in maximum lift coefficient to 9.1. This is larger than the potential flow limit for this particular airfoil, which is the basis for the "Superlift Coefficient" definition. The larger leading edge radius of NASA SC(2)-0714 compared to NASA SC(2)-1010 and RAE-2822 appears to correlate to being able to reach higher angles of attack. Similarly, NASA SC(2)-1010, while thinner than RAE-2822, has a larger radius at the leading edge and is able to reach a higher maximum lift coefficient of 5.9. The potential flow limit is dependent on airfoil thickness, but seems to be less of a factor in reality for supercritical airfoils.

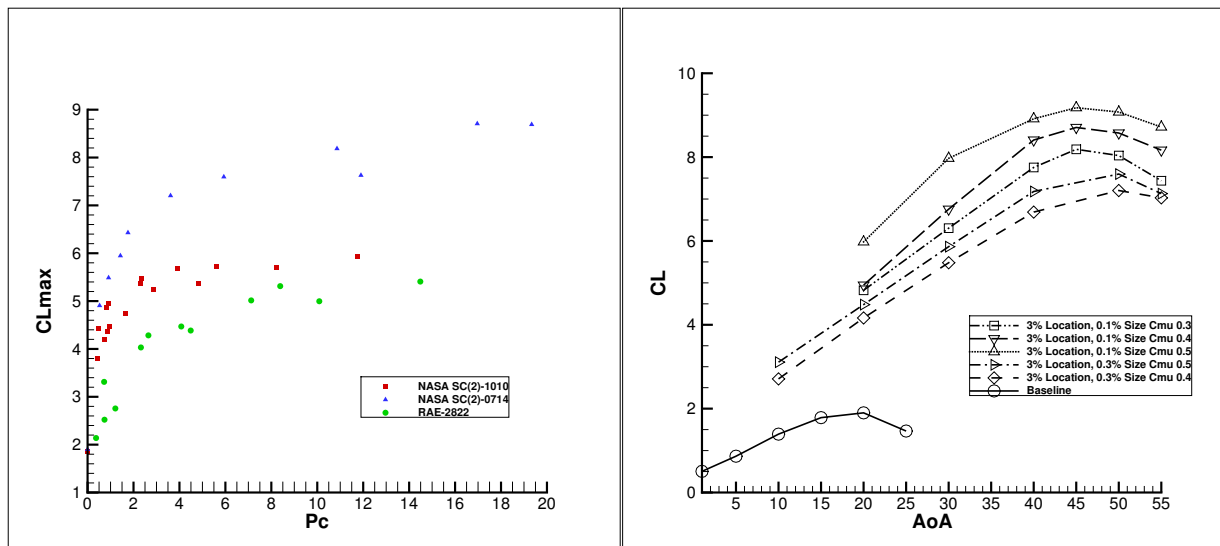


Figure 35: (A) Maximum Lift Coefficient for Various Configurations v Power Coefficient
(B) NASA SC(2)-0714 Lift Coefficient

The maximum lift coefficient for each power coefficient forms a logarithmic curve. This appears to be independent of injection configuration; the power coefficient appears to directly relate to maximum lift coefficient. The exact nature of these curves warrant further study. By injecting the jet at low pressure, and sucking the flow in at high relative pressure the best liftoff and takeoff configuration provides a benefit at cruise due to low power consumption. CFJ supercritical airfoils therefore, provide a simpler alternative to current multi-element ESTOL systems, while possibly reducing weight and providing superior performance at low-speed and cruise.

V. Acknowledgments

This project is sponsored by the Defense Advanced Research Projects Agency and monitored by the program manager Jean-Charles Ledé under Cooperative Agreement No.: HR0011-16-2-0052. The content of the information does not necessarily reflect the position or the policy of the Government, and no official endorsement should be inferred. The simulations are conducted on Pegasus supercomputing system at the Center for Computational Sciences at the University of Miami.

References

- ¹ R. T. Whitcomb and L. R. Clark. An Airfoil Shape for Efficient Flight at Supercritical Mach Numbers. *NASA TM*, X-1109, 1965.
- ² Liu, Z.-X. and Zha, G.-C. Transonic Airfoil Performance Enhancement Using Co-Flow Jet Active Flow Control. AIAA Paper 2016-3472, AIAA AVIATION 2016, 8th AIAA Flow Control Conference, Washington, D.C, June 13-17, 2016.
- ³ Yang, Y.-C. and Zha, G.-C. Super-Lift Coefficient of Active Flow Control Airfoil: What Is the Limit? AIAA Paper 2017-1693, AIAA SCITECH2017, 55th AIAA Aerospace Science Meeting, Grapevine, Texas, 9-13 January 2017.
- ⁴ Rudolph, P. K. C. High-Lift Systems on Commercial Subsonic Airliners. NASA Contractor Report 4746, Sept. 1996.
- ⁵ C.D. Harris. NASA Supercritical Airfoils. *NASA Technical Paper*, 2969, 1990.
- ⁶ Corke, T. C. *Design of Aircraft*. Prentice Hall, 2003.
- ⁷ G.-C. Zha and D. C. Paxton. A Novel Flow Control Method for Airfoil Performance Enhancement Using Co-Flow Jet. *Applications of Circulation Control Technologies*, Chapter 10, p. 293-314, Vol. 214, Progress in Astronautics and Aeronautics, AIAA Book Series, Editors: Joslin, R. D. and Jones, G.S., 2006.
- ⁸ G.-C Zha and C. Paxton and A. Conley and A. Wells and B. Carroll. Effect of Injection Slot Size on High Performance Co-Flow Jet Airfoil. *AIAA Journal*, 43, 2006.
- ⁹ G.-C. Zha and W. Gao and C. Paxton. Jet Effects on Co-Flow Jet Airfoil Performance. *AIAA Journal*, No. 6, 45:1222–1231, 2007.
- ¹⁰ G.-C Zha and B. Carroll and C. Paxton and A. Conley and A. Wells. High Performance Airfoil with Co-Flow Jet Flow Control. *AIAA Journal*, 45, 2007.
- ¹¹ Wang, B.-Y. and Haddoukessouni, B. and Levy, J. and Zha, G.-C. Numerical Investigations of Injection Slot Size Effect on the Performance of Co-Flow Jet Airfoil . *AIAA Journal of Aircraft*, 45:2084–2091, 2008.
- ¹² B. P. E. Dano, D. Kirk, and G.-C. Zha. Experimental Investigation of Jet Mixing Mechanism of Co-Flow Jet Airfoil. AIAA Paper 2010-4421, 5th AIAA Flow Control Conference, Chicago, IL., 28 Jun - 1 Jul 2010.
- ¹³ B. P. E. Dano, G.-C. Zha, and M. Castillo. Experimental Study of Co-Flow Jet Airfoil Performance Enhancement Using Micro Discreet Jets. AIAA Paper 2011-0941, 49th AIAA Aerospace Sciences Meeting, Orlando, FL., 4-7 January 2011.
- ¹⁴ Lefebvre, A. and Dano, B. and Di Franzo, M. and Bartow, W. and Zha, G.-C. Performance of Co-Flow Jet Flow Airfoil with Variation of Mach Number. AIAA Paper 2013-0490, 51st AIAA Aerospace Science Meeting, Grapevine, TX, 7-10 Jan. 2013, to appear in *Journal of Aircraft*, 2016.
- ¹⁵ Lefebvre, A. and Zha, G.-C. Numerical Simulation of Pitching Airfoil Performance Enhancement Using Co-Flow Jet Flow Control. AIAA Paper 2013-2517, 31st AIAA Applied Aerodynamics Conference, San Diego, CA, 24 - 27 June 2013.
- ¹⁶ Lefebvre, A. and Zha, G.-C. . Design of High Wing Loading Compact Electric Airplane Utilizing Co-Flow Jet Flow Control. AIAA Paper 2015-0772, AIAA SciTech2015: 53nd Aerospace Sciences Meeting, Kissimmee, FL, 5-9 Jan 2015.
- ¹⁷ Lefebvre, A. and Dano, B. and Bartow, W. and Di Franzo, M. and Zha, G.-C. Performance and Energy Expenditure of Co-Flow Jet Airfoil with Variation of Mach Number. *AIAA Journal of Aircraft*, 53:1757–1767, 2016.
- ¹⁸ P.R. Spalart and S.R. Allmaras. A One-equation Turbulence Model for Aerodynamic Flows. AIAA-92-0439, 1992.

- ¹⁹ G.-C. Zha, Y. Shen, and B. Wang. An improved low diffusion E-CUSP upwind scheme . *Journal of Computer & Fluids*, 48:214–220, 2011.
- ²⁰ P. Roe. Approximate Riemann Solvers, Parameter Vectors, and Difference Schemes. *Journal of Computational Physics*, 43:357–372, 1981.
- ²¹ Shen, Y.-Q. and Zha, G.-C. and Wang, B.-Y. Improvement of Stability and Accuracy of Implicit WENO Scheme. *AIAA Journal*, 47, No. 2:331–344, 2009.
- ²² Shen, Y.-Q. and Zha, G.-C. and Chen, X.-Y. High Order Conservative Differencing for Viscous Terms and the Application to Vortex-Induced Vibration Flows. *Journal of Computational Physics*, 228(2):8283–8300, 2009.
- ²³ Y.-Q. Shen, B.-Y. Wang, and G.-C. Zha. Implicit WENO Scheme and High Order Viscous Formulas for Compressible Flows . AIAA Paper 2007-4431, 2007.
- ²⁴ B.-Y. Wang and G.-C. Zha. A General Sub-Domain Boundary Mapping Procedure For Structured Grid CFD Parallel Computation. *AIAA Journal of Aerospace Computing, Information, and Communication*, 5, No.11:2084–2091, 2008.
- ²⁵ Hu, Z.-J. PARALLEL COMPUTATION OF FLUID-STRUCTURAL INTERACTIONS USING HIGH RESOLUTION UPWIND SCHEMES. Ph.D. Thesis, University of Miami, Dept. of Mechanical and Aerospace Engineering, May 2005.
- ²⁶ Y.-Q. Shen and G.-C. Zha. Comparison of High Order Schemes for Large Eddy Simulation of Circular Cylinder Flow. AIAA-2009-0945, 47th AIAA Aerospace Sciences Meeting and Exhibit, Orlando, FL, Jan. 5-8, 2009.
- ²⁷ Y.-Q. Shen J.-Y. Gan and G.-C. Zha. Comparison of Drag Prediction Using RANS models and DDES for the DLR-F6 Configuration Using High Order Schemes. 54th Aerospace Sciences Meeting, San Diego, CA, AIAA Paper 2016-0553, 2016.
- ²⁸ Rivers, Melissa B., Wahls, Richard A. Comparison of Computational and Experimental Results for a Supercritical Airfoil . NASA Technical Memorandum 4601, November, 1994.